THE ASTROPHYSICAL JOURNAL, 348:253–278, 1990 January 1

EINSTEIN OBSERVATORY MAGNITUDE-LIMITED X-RAY SURVEY OF LATE-TYPE GIANT AND SUPERGIANT STARS

A. MAGGIO AND G. S. VAIANA[1]
Osservatorio Astronomico di Palermo
B. M. HAISCH AND R. A. STERN
Lockheed Palo Alto Research Laboratory
J. BOOKBINDER
JILA, University of Colorado, and Smithsonian Astrophysical Observatory
F. R. HARNDEN, JR.
Harvard-Smithsonian Center for Astrophysics
AND
R. ROSNER
Department of Astronomy and Astrophysics and Enrico Fermi Institute, University of Chicago
Received 1988 October 3; accepted 1989 July 1

ABSTRACT

We present results of an extensive X-ray survey of 380 giant and supergiant stars of spectral types from F to M carried out with the *Einstein Observatory*. Taking into account the sample limited to visual magnitude $m_v < 6.3$, we find that more than 40% of the observed F and G giants have been detected, both in the total sample and in the single star sample. Among the K giants, 14% have been detected (all of them early K), but most of the X-ray sources have been identified with RS CVn–type or multiple systems, and only two detections (4%) refer to single stars. None of the 29 M giants have been detected, except for one spectroscopic binary. Finally, we report seven detections out of 46 bright giants or supergiants observed (luminosity classes II or I), only one of the sources being a single star (α Car, F0 II). Using both detections and upper limits, we derive stellar X-ray luminosity functions in the energy range (0.2–4) keV for different spectral types and compare these with luminosity functions previously obtained for main-sequence stars. We find a statistically significant drop in the number of detections at spectral type K ($B-V \sim 1.1$). This drop, already known as the X-ray dividing line, is now established on a firm statistical ground and not simply as a suggestion based on limited samples. We are in no position to explore with equivalent statistical certainty a luminosity class dependence of such a drop. However, within the more limited statistics, the X-ray luminosity function of the class I and II stars as a whole cannot be distinguished from that of the class III stars in our sample. The X-ray emission drop seems to be associated with the ascending phase of the red giant branch. We also stress the presence of many RS CVn systems near the X-ray dividing line, with an emission level comparable to that of presumed single giant stars of similar spectral type. The detection of X-ray emission from G giants with masses $M \gtrsim 2\ M_\odot$ (presumably spectral type A on the main sequence) suggests that the onset of a convective envelope may be the triggering ingredient of an efficient dynamo mechanism during the approach to the red giant branch. We find within this sample a poor correlation between the X-ray luminosity and the projected rotational velocity; this occurrence suggests that additional parameters are needed to characterize the stellar dynamo for the giants on the active side of the H-R diagram. The internal differential rotation and the depth of the convective zone are the most probable ingredients for this purpose.

Subject headings: stars: coronae — stars: X-rays — X-rays: sources

I. INTRODUCTION

The X-ray data provided by the *Einstein Observatory* satellite have been extensively used in past years to build a comprehensive picture of the high-energy emission from stars throughout the H-R diagram (see Rosner, Golub, and Vaiana 1985; Haisch 1986; Vaiana and Sciortino 1986 for the most recent reviews) and, by inference, to map the occurrence of hot plasma in stellar atmospheres. In this picture, one of the most interesting and puzzling roles is played by the evolved late-type stars. In the first survey of ultraviolet emission spectra of late-type stars using the *International Ultraviolet Explorer* (*IUE*) satellite, Linsky and Haisch (1979) proposed the existence of a sharp dividing line in the H-R diagram, separating solar-type and non–solar-type stars. The first group comprises main-sequence and giant stars which exhibit a solar-like chromospheric ($T \sim 10^4$ K) and transition region ($T \sim 10^5$ K) emission-line spectrum, while the non–solar-type group consists of giants cooler than about spectral type K2 III, and of late G–M supergiants which show only a chromospheric spectrum, with no evidence of plasma hotter than ~ 1–2×10^4 K. Following the solar analogy, the presence of a transition region implies the existence of an upper atmospheric layer (corona) where the plasma temperature reaches $\sim 10^6$ K and soft X-ray emission originates. In fact, Vaiana *et al.* (1981) and Ayres *et al.* (1981) reported the detection of soft X-ray emission from late F through early K giants, but not from cooler single giants or

[1] Also Harvard-Smithsonian Center for Astrophysics and IAIF-CNR.

from any supergiants other than α Car (F0 Ib–II). Moreover, among the luminous cool stars to the left of the boundary, Ayres *et al.* observed a range in coronal emission of more than two orders of magnitude. This result was based on a sample of about 30 giant and supergiant stars observed with the *Einstein Observatory* and was confirmed by Haisch and Simon (1982) using the observations of eight more G–K giant stars. More recently, the sample of evolved stars observed in the X-ray region has increased slightly, thanks to the publication of few more *Einstein Observatory* measurements (Haisch 1987) and a few new *EXOSAT* observations (Gondoin, Mangenay, and Praderie 1987). Because of the small number of cases examined and the uneven sampling mode, X-ray luminosity functions for giants and supergiants have never been computed up to date. The first goal of our work is to accomplish this task using a complete matnitude-limited star sample. A further goal is to verify whether stellar parameters, such as surface rotation rate and age, are still helpful in distinguishing strong from weak coronal X-ray sources on the active side of the H-R diagram, as in the case of late-type dwarf stars. Finally, it is not clear how far the solar analogy can be pushed to explain the varied activity regimes of the giant and supergiant stars near the transition region dividing line (TRDL) introduced by Linsky and Haisch (1979).

Any interpretation of the lack of UV and X-ray emission on the cool side of the TRDL should take into account the presence of other "discontinuities" in stellar physical properties observed in the same region of the H-R diagram. The TRDL shows, in fact, an intriguing qualitative correlation with the locus where the onset of massive stellar winds takes place. The observational evidence for such a locus rests on the appearance of circumstellar absorption features in the Ca II H and K lines (Reimers 1977), and also on a statistical difference in the asymmetry of the doubly peaked Ca II K and Mg II *k* lines (Stencel 1978; Stencel and Mullan 1980). Moreover, Gray (1982) has called attention to a sudden drop in the surface rotational velocities of stars later than G5 III, which seems to require a strong external brake, such as is applied by a magnetically coupled stellar wind (Endal 1983; see, however, Rutten and Pylyser 1988). The question now arises whether the transition to a nonsolar behavior of the stars on the left of the TRDL is linked in terms of cause and effect to any of the other boundary lines. From a different point of view, we are interested in understanding if this transition is the result of a natural evolutionary aging of a magnetic dynamo mechanism (Ayres *et al.* 1981), such as the one which powers the solar corona, or if we have to invoke a different explanation. In particular, alternative scenarios have been proposed following the observation that stars on either side of the TRDL have different surface gravities. In fact, the energy balance in the outer atmospheres may drastically change because of the onset of strong winds (Linsky and Haisch 1979), the occurrence of radiative instabilities (Simon, Linsky, and Stencel 1982), or the development of widely extended chromospheres (Böhm-Vitense 1986). Finally, Antiochos, Haisch, and Stern (1986) have shown that an increase in the gravitational scale height may result in a thermal instability of hot ($T \sim 10^6$ K) coronal structures, so that preference is given to cool ($T \sim 10^4$ K) solutions of the static loop equations for sufficiently small surface gravities (Antiochos and Noci 1986). The X-ray survey we have carried out is extended to all the late-type evolved stars listed in *The Bright Star Catalogue* (BSC) (Hoffleit and Jaschek 1982) and observed by the *Einstein Observatory*. Because of the inclusion of both pointed and serendipitous observations, the sample we present in this paper is about 10 times larger than any previously studied sample, and we are now in the position to definitely establish whether the X-ray emission regime changes upon crossing the TRDL.

This paper is organized as follows. In § II, we explain our selection criteria and the composition of our X-ray sample; in § III, the X-ray data processing is described; § IV and § V are devoted to results and a discussion, and § VI contains a brief summary.

II. THE SURVEY SAMPLE

a) Selection Criteria

We have selected all the optical candidates in the BSC and its supplement (Hoffleit, Saladyga, and Wlasuk 1984), with luminosity classes III or brighter and spectral types in the range F to M. Of the 4168 optically selected stars, 380 fell into one of the *Einstein Observatory* imaging proportional counter fields of view and form the observed sample. The composition of these samples with respect to spectral types and luminosity classes is shown in Table 1, while the observed stars are listed in Table 2 with relevant optical properties.

Bahcall, Casertano, and Ratnatunga (1987) show that the BSC is complete to apparent visual magnitude $m_v \sim 6.3$. We have confirmed this finding also for our optical population: in Figure 1, we show the m_v integral distribution function for all the optical candidates (*solid line*) and note that no flattening occurs for $m_v < 6.3$ (279 stars in our observed sample meet this criterion). We have also checked the completeness of the subsample of stars with measured and reliable trigonometric parallaxes ($\pi > 0.01$): the corresponding log N–m_v curve (*dotted line* in Fig. 1) now flattens for $m_v \gtrsim 5$; therefore, we have restricted our attention to the 98 stars with distance $D < 100$ pc and $m_v < 5$ in order to build the X-ray luminosity functions (see § IV).

In summary, the *Einstein Observatory* satellite observed ~9% of all the giant and supergiant stars listed in the BSC. In the following, we will call "giants" all stars with luminosity class III–IV, III, or II–III, and we will call all the others "supergiants".

b) Sample Properties

In Figure 2, we show the H-R diagram (absolute visual magnitude M_v vs. $B-V$ color) for all the stars in the observed

TABLE 1

SURVEY STATISTICS

SPECTRAL TYPE	FULL SAMPLE			SINGLE STAR SAMPLE	
	Optical	Observed	Detected	Observed	Detected
Giants (luminosity classes III–IV, III, and II–III)					
F	255	25	9	10	3
G	810	85	32	38	12
K	2009	163	20	85	2
M	607	45	1	26	0
Supergiants (luminosity classes II, I–II, and I)					
F	124	18	2	7	1
G	166	22	4	9	0
K	153	16	1	8	0
M	44	5	0	4	0

TABLE 2

OPTICAL PROPERTIES OF THE SAMPLE STARS, X-RAY DATA, AND ROTATIONAL VELOCITIES

HR	HD	Name[a]	Spectral Type	B-V	m_v	M_v	Parallax (")	Flag[b]	Journal of Observations[c]	f_x[d] (10^{-13} erg cm^{-2} s^{-1})	Δf_x[d]	log f_x/f_v	log L_x	v sin$i$ ($km\ s^{-1}$)	Ref.
			Giants (luminosity classes III-IV, III, and II-III)												
3	28	33 Psc	K1III	1.04	4.61	0.3	0.014	R *	8019 222 1	< 1.6	...	< -5.4	< 29.0	< 17	1
14	352	.....	K2III	1.38	6.07	...	...	M *	9062 544 1	1.8	0.6	-4.8	...	...	
21	432	β Cas	F2III-IV	0.34	2.27	1.6	0.072	M *	2244 1 1	6.8	1.6	-5.8	28.2	70	1
...	1563	91850	gG8	0.98	6.61	...	...	S	3457 S 1	2.2	0.5	-4.5	...	...	
...	2901	21506	K2III*	1.25	6.89	...	...	S	5178 S 1	< 2.6	...	< -4.3	...	...	
163	3546	ϵ And	G8IIIp	0.87	4.37	2.2	0.037	S *	7697 322 2	< 1.3	...	< -5.6	< 28.1	9	1
167	3690	55 Psc	K0III+F3V	1.16	5.36	0.1	0.009	M *	7640 S 2	< 1.4	...	< -5.2	...	...	
177	3856	.....	G9III-IV	1.04	5.83	...	...	S *	3628 S 1	< 1.8	...	< -4.9	...	...	
188	4128	β Cet	K0IIICH-1H K-0.5	1.02	2.04	1.0	0.061	S *	4452 208 1	168.4	6.9	-4.5	29.7	3	2
236	4815	λ Hyi	K5III	1.37	5.07	2.1	0.025	M *	595 S 1	< 9.4	...	< -4.5	< 29.3	...	
259	5316	.....	M4IIIab	1.62	6.20	...	...	S *	5988 S 1	< 1.7	...	< -4.8	...	...	
271	5516	η And	G8IIIb	0.94	4.42	-0.8	0.009	M *	4940 227 1	41.2	5.2	-4.1	...	< 17	1
339	6903	ψ^3 Psc	G0III	0.69	5.55	...	...	S *	10105 626 1	3.8	1	-4.7	...	91	1
344	6966	.....	M0III	1.49	6.06	...	...	M *	194 S 1	< 2.9	...	< -4.6	...	...	
347	7014	33 Cet	K4III	1.51	5.95	...	...	S *	8458 S 1	< 1.5	...	< -4.9	...	...	
371	7578	.....	K1III	1.15	6.02	...	...	S *	6703 2 1	< 1.4	...	< -4.9	...	...	
373	7672	39 Cet	G5IIIe	0.90	5.41	1.3	0.015	R *	3192 54 1	416.6	12.5	-2.7	31.3	...	
392	8334	.....	K5IIIab	1.52	6.20	...	...	M *	153 S 1	< 2.7	...	< -4.6	...	...	
407	8634	.....	F5III	0.43	6.18	...	...	M *	7431 3 1	6	1.8	-4.2	...	34	1
414	8763	94 Psc	K1III	1.11	5.50	1.1	0.013	M *	6080 S 2	< 1.2	...	< -5.2	< 28.9	...	
426	8949	.....	K1III	1.12	6.20	...	...	M *	454 S 1	< 3.3	...	< -4.5	...	...	
469	10072	χ And	G8III	0.89	4.98	-0.2	0.009	M *	4941 227 1	15.3	2.4	-4.3	...	< 17	1
547	11522	.....	F0IIIn	0.27	5.80	...	...	S *	2481 S 1	< 7.2	...	< -4.3	...	...	
587	12292	.....	M3III	1.52	5.51	...	...	M *	5163 S 1	< 3	...	< -4.8	...	...	
617	12929	α Ari	K2IIIabCa-I	1.15	2.00	0.5	0.049	M *	852 0 1	< 0.7	...	< -6.8	< 27.6	3.1	2
621	13137	.....	G8III	0.95	6.31	...	...	S	1239 S 1	< 1.9	...	< -4.7	...	...	
626	13222	.....	G8III	0.91	6.29	...	...	M *	10235 S 1	1.8	0.4	-4.7	...	...	
642	13480	6 Tri	G5III+F5V	0.78	4.94	-2.1	0.004	R *	3533 99 1	95.4	5.7	-3.5	...	36	1
681	14386	o Cet	M7IIIe	1.42	3.04	-0.1	0.024	M *	2253 1 1	< 1.4	...	< -6.1	< 28.5	...	
...	14914	23327	K0III/IV	...	6.98	...	...	S	5074 S 1	< 1.5	...	< -4.5	...	...	
738	15755	.....	K0III	1.07	5.83	...	...	M *	5142 S 1	< 1.1	...	< -5.1	...	...	
...	16446	167931	gG9	1.08	6.78	...	...	S	2013 S 2	< 1.9	...	< -4.5	...	...	
844	17713	γ^1 For	K1III	1.07	6.14	...	...	M *	6128 S 1	< 3.8	...	< -4.5	...	...	
862	18071	.....	K0III	1.04	5.95	...	...	S *	6730 S 1	< 3.3	...	< -4.6	...	...	
911	18884	α Cet	M1.5IIIa	1.64	2.53	-2.7	0.009	S *	5450 0 1	< 0.7	...	< -6.6	...	...	
946	19637	.....	K3III	1.28	6.02	...	...	S *	835 S 1	< 4.2	...	< -4.5	...	...	
949	19735	.....	K5III	1.43	6.33	...	...	M	3193 S 1	< 2.8	...	< -4.5	...	...	
956	19845	.....	G9III	0.97	5.90	...	...	S *	3193 S 1	< 2.1	...	< -4.8	...	...	
1007	20791	κ^2 Cet	G8.5III	0.97	5.69	...	...	M *	7955 S 1	< 1.1	...	< -5.2	...	< 15	3
1008	20794	.....	G8III	0.71	4.27	5.3	0.162	S *	3105 994 1	< 2	...	< -5.5	< 27.0	...	
1132	23183	14 Tau	G8III	1.01	6.14	...	...	M *	9258 1 1	< 1.7	...	< -4.8	...	...	
1168	23697	.....	K1III	1.04	6.30	...	...	M	3437 S 1	< 5.8	...	< -4.2	...	...	
1256	25604	37 Tau	K0III	1.07	4.36	-0.1	0.013	S *	7918 385 1	< 1	...	< -5.7	< 28.9	< 17	1
1265	25723	.....	gK0	1.08	5.61	...	...	M *	9528 S 2	< 2.5	...	< -4.9	...	...	
1336	27256	α Ret	G8II-III	0.91	3.35	-1.1	0.013	M *	5166 S 2	17.6	0.9	-4.9	30.1	...	

TABLE 2—*Continued*

HR	HD	Name[a]	Spectral Type	B-V	m_v	M_v	Parallax (")	Flag[b]	Journal of Observations[c]		f_x[d] (10^{-13} erg cm^{-2} s^{-1})	Δf_x[d]	log f_x/f_v	log L_x	v sin$i$ ($km\ s^{-1}$)	Ref.
1337	27278	.....	K0III	0.94	5.92	...	...	M *	5054	S 1	< 10.4	...	< -4.1	...	...	
1346	27371	γ Tau	K0-IIIabCN1	0.99	3.65	0.9	0.028	M *	3663	S 2	14.6	1.3	-4.9	29.3	2.4	2
1373	27697	δ^1 Tau	K0IIICN0.5	0.98	3.76	0.4	0.021	M *	3668	S 2	4.3	1.1	-5.4	29.1	2.5	2
1396	28100	π Tau	G7IIIaFe-1	0.98	4.69	0.4	0.014	S *	3523	S 2	< 4.4	...	< -5.0	< 29.4	< 17	1
1407	28292	75 Tau	K2IIIv	1.13	4.97	...	...	M *	9006	S 4	< 1.9	...	< -5.2	...	< 19	1
1411	28307	θ^1 Tau	K0IIIbFe-0.5	0.95	3.84	1.7	0.038	M *	9005	519 3	29.1	1.3	-4.5	29.4	3.4	2
...	28595	93983	M3III	1.70	6.34	...	...	S	3525	S 1	< 1.4	...	< -4.8	...	...	
1454	29094	58 Per	K4III+A3V	1.22	4.25	0.3	0.016	M *	4228	1 1	< 1.6	...	< -5.6	< 28.9	6.3	4
1457	29139	α Tau	K5III	1.54	0.85	-0.5	0.054	M *	4451	208 1	< 2.6	...	< -6.8	< 28.0	2.7	5
1467	29317	3 Cam	K0III	1.07	5.05	...	...	M *	4942	227 1	13.1	1.5	-4.4	...	< 17	1
1562	31139	5 Ori	M1III	1.64	5.33	0.3	0.010	S *	5025	S 1	< 2	...	< -5.1	...	...	
1623	32357	12 Cam	K0III	...	6.25	...	...	R *	3196	54 1	51.2	4.2	-3.3	...	< 25	1
1708	34029	α Aur	G5IIIe+G0III	0.80	0.08	-0.4	0.080	R *	849	0 1	1338.2	26.7	-4.3	30.4	...	
1744	34649	θ Dor	K2.5IIIa	1.28	4.83	...	...	M *	6302	S 2	< 4	...	< -5.0	...	...	
1816	35802	117 Tau	M1III	1.63	5.77	...	...	S *	3532	S 1	< 2.7	...	< -4.8	...	...	
1867	36689	.....	K4-5III	1.53	6.59	...	...	S	9025	S 1	< 9.8	...	< -3.9	...	...	
1901	37077	45 Ori	F0III	0.24	5.26	2.3	0.026	M *	9256	S 2	< 5	...	< -4.7	< 28.9	66	1
1970	38099	.....	K4III	1.47	6.31	...	...	M	9061	544 1	< 1.1	...	< -4.9	...	...	
2030	39286	.....	B8III+G2IIIe	0.54	6.06	...	...	M *	4347	S 1	85.1	7.8	-3.1	...	50	1
2063	39816	.....	M6.5IIIe	...	5.40	...	...	S *	4347	S 1	< 2.8	...	< -4.9	...	...	
2070	39910	.....	gK2	1.18	5.87	...	...	S *	3109	S 1	< 1.9	...	< -4.9	...	...	
2085	40136	η Lep	F1III	0.33	3.71	2.8	0.066	S *	5482	0 1	12	2.1	-4.9	28.5	...	
...	40280	77800	K0III	0.99	6.60	...	...	S	5065	S 2	< 1.5	...	< -4.7	...	...	
2134	41116	1 Gem	G7III	0.82	4.16	1.6	0.031	M *	5183	222 1	2.1	0.5	-5.5	28.4	...	
2216	42995	η Gem	M3III	1.60	3.28	-1.0	0.014	M *	5928	S 2	4.4	0.9	-5.5	29.4	...	
2322	45291	.....	G8III	1.04	5.98	...	...	S *	6960	S 1	< 2	...	< -4.8	...	...	
2341	45509	.....	K5-M0III	1.70	6.51	...	...	S	6960	S 2	< 0.9	...	< -5.0	...	...	
2553	50310	τ Pup	K1III	1.20	2.93	...	...	M *	5488	0 1	< 1.3	...	< -6.2	...	< 15	3
2574	50778	θ CMa	K4III	1.43	4.07	0.8	0.022	S *	7921	385 1	< 1.1	...	< -5.8	< 28.4	< 19	1
2590	51199	π CMa	gF2	0.37	4.68	2.3	0.034	M *	7898	S 1	3.6	1	-5.1	28.6	120	1
2634	52603	.....	K2III	1.16	6.27	...	...	S *	9961	S 1	< 2.2	...	< -4.7	...	...	
2639	52666	.....	M2III	1.68	5.20	...	...	M *	3335	S 1	< 1.7	...	< -5.2	...	...	
2655	53208	.....	K3III	1.29	5.62	...	...	M *	3198	S 1	< 1.9	...	< -5.0	...	...	
2670	53755	.....	B0.5V+F5III	-0.05	6.49	...	...	M	5035	S 1	< 3.9	...	< -4.3	...	412	1
2750	56160	.....	K4III	1.22	5.58	...	...	M *	5495	S 1	11.5	3.5	-4.2	...	...	
2771	56813	.....	K4III	1.44	5.66	...	...	S *	5494	S 1	< 1.4	...	< -5.1	...	...	
2938	61338	74 Gem	K5IIIFe-0.5	1.56	5.05	-0.2	0.009	M *	5695	S 4	< 3.4	...	< -4.9	...	...	
2973	62044	σ Gem	K1III	1.12	4.28	0.6	0.018	R *	2311	1 2	427.4	8.2	-3.2	31.2	22	1
2975	62066	51 Cam	gK2	1.18	5.92	...	...	S *	2653	S 1	< 4.1	...	< -4.5	...	...	
2990	62509	β Gem	K0IIIb	1.00	1.14	1.0	0.094	M *	4453	208 1	3.1	0.8	-6.5	27.6	2.5	2
3043	63660	.....	G0III	0.76	5.33	3.1	0.036	M *	7866	S 1	< 1.2	...	< -5.3	< 28.1	...	
...	64259	153522	K2III	1.11	6.61	...	...	M	10669	S 1	< 1.5	...	< -4.7	...	...	
...	64616	174755	K0III	0.93	6.92	...	...	S	4235	S 1	< 1.1	...	< -4.7	...	...	
...	64657	174762	M5/6III	1.55	6.85	...	...	S	4235	S 1	< 0.9	...	< -4.8	...	...	
...	66676	219343	K1III	...	6.99	...	...	S	2223	S 5	< 2.5	...	< -4.3	...	...	
3175	67224	.....	gK4	...	5.94	...	...	S *	7778	S 1	< 3.8	...	< -4.5	...	...	
...	69066	198967	G4III	0.79	6.89	...	...	S	1752	S 1	< 3.1	...	< -4.2	...	...	

TABLE 2—*Continued*

HR	HD	Name[a]	Spectral Type	B-V	m_v	M_v	Parallax (")	Flag[b]	Journal of Observations[c]	f_x[d] (10^{-13} erg cm^{-2} s^{-1})	Δf_x[d]	log f_x/f_v	log L_x	v sin$i$ (km s^{-1})	Ref.
3242	69123	.....	K1III	1.02	5.78	...	...	S *	1752 S 1	< 2.2	...	< -4.8	...	...	
3264	69994	.....	K1III	1.13	5.83	...	...	M *	304 S 1	< 1	...	< -5.2	...	...	
...	70195	219772	G8/K0III	0.96	7.07	...	...	S	3754 S 1	< 3.4	...	< -4.1	...	...	
3289	70673	22 Pup	gG7	1.00	6.11	...	...	S *	551 S 1	< 3.9	...	< -4.5	...	...	
3307	71129	ϵ Car	K3III+B2:V	1.28	1.86	...	...	M *	5501 0 1	< 2.1	...	< -6.4	...	...	
3318	71243	α Cha	F5III	0.39	4.07	2.7	0.053	S *	10100 626 1	13.2	2	-4.8	28.7	36	1
3355	72041	υ^1 Cnc	F0IIIn	0.28	5.75	...	...	M *	3264 S 1	< 2	...	< -4.9	...	97	1
...	72066	219981	K3/4III:	1.39	6.75	...	...	S	8033 S 1	< 6	...	< -4.0	...	...	
3390	72900	.....	K3III	1.56	6.24	...	...	S *	746 S 1	< 13.1	...	< -3.9	...	...	
3403	73108	π^2 UMa	K1IIIbCN-0.5	1.17	4.60	0.6	0.016	S *	6964 S 1	< 2.8	...	< -5.2	< 29.1	< 17	1
3423	73596	.....	F5III	...	6.10	...	...	M *	3204 S 1	< 2.7	...	< -4.6	...	...	
3431	73840	6 Hya	K4III	1.42	4.98	1.8	0.023	S *	8933 S 1	< 1.5	...	< -5.3	< 28.5	< 19	1
3444	74167	.....	M0III	1.65	5.71	...	...	S *	735 S 1	< 5	...	< -4.5	...	...	
...	74599	220339	K3III	1.51	6.84	...	...	S	736 S 1	< 5.3	...	< -4.0	...	...	
3477	74772	.....	G5III	0.87	4.07	2.6	0.051	M *	722 S 1	< 29.7	...	< -4.4	< 29.1	...	
3521	75716	53 Cnc	M3III	1.62	6.23	-3.8	0.001	M *	5504 S 1	< 0.6	...	< -5.2	...	...	
3547	76294	ζ Hya	G9II-III	1.00	3.11	0.8	0.035	S *	5506 0 1	< 1.8	...	< -6.0	< 28.2	< 1.4	4
3577	76830	.....	M4IIIv	1.55	6.38	...	...	S	3356 S 1	< 4.8	...	< -4.3	...	...	
...	80060	250505	K0III	1.07	7.06	...	...	S	6404 S 1	< 4.8	...	< -4.0	...	...	
...	80105	155064	gG6	1.03	7.07	...	...	S	1894 S 1	< 1	...	< -4.7	...	...	
3706	80499	26 Hya	G8III	0.93	4.79	1.6	0.023	M *	1894 S 1	< 1.3	...	< -5.5	< 28.5	< 19	1
...	81192	80809	G7III+ dG5	0.94	6.56	...	...	M	5365 S 1	< 1.9	...	< -4.6	...	...	
...	81353	236913	G8II/III	1.05	6.81	...	...	M	5309 S 1	< 2.4	...	< -4.4	...	...	
3748	81797	α Hya	K3II-III	1.44	1.98	-1.3	0.022	M *	853 0 1	< 2	...	< -6.4	< 28.7	< 1.4	4
3771	82210	24 UMa	G4III-IV	0.77	4.56	2.7	0.042	S *	3535 99 1	129.8	6	-3.6	29.9	4.9	6
...	83564	27340	K1III/IV	1.13	6.50	...	...	S	3368 S 1	< 4.6	...	< -4.2	...	...	
3851	83805	43 Lyn	G8III	0.95	5.62	1.9	0.018	S *	4621 S 1	< 1.4	...	< -5.1	< 28.7	< 19	1
3903	85444	υ^1 Hya	G7-III-IIIb	0.92	4.12	0.7	0.021	S *	7607 S 1	28.7	2.4	-4.4	29.9	< 19	1
...	86778	81143	K2III	...	6.94	...	...	S	2687 S 1	< 1.9	...	< -4.5	...	...	
...	87806	118120	gM2	...	6.65	...	...	S	7406 S 1	< 2.2	...	< -4.5	...	...	
3994	88284	λ Hya	K0IIICN1	1.01	3.61	0.8	0.027	M *	9696 S 1	< 1.5	...	< -5.9	< 28.4	< 19	1
4057	89484	γ^1 Leo	K1-IIIbCN-0.5	1.15	2.61	-0.7	0.022	M *	913 S 1	< 1	...	< -6.5	< 28.4	2.6	2
4058	89485	γ^2 Leo	G7IIICN-I	...	3.80	0.5	0.022	M *	913 S 1	< 1	...	< -6.0	< 28.4	2.7	2
4091	90289	.....	K4III	1.52	6.35	...	...	S	7715 S 2	< 1.2	...	< -4.9	...	...	
...	90512	99132	G5III	0.85	6.66	...	...	S	7701 S 1	< 4.5	...	< -4.2	...	< 20	1
...	90861	81381	K2III	1.12	6.90	...	...	S	2644 S 1	< 2.6	...	< -4.3	...	...	
...	90980	238102	K0III	1.02	6.74	...	...	S	3340 S 1	< 2.1	...	< -4.5	...	...	
4162	92036	.....	M2III	1.62	4.89	-0.1	0.010	S *	6114 S 1	< 1.9	...	< -5.3	...	...	
4165	92095	.....	K3III	1.27	5.52	...	...	S *	467 S 1	< 1.9	...	< -5.0	...	...	
4200	93070	.....	K4III	1.71	4.57	1.1	0.020	M *	4223 S 1	< 3.1	...	< -5.2	< 29.0	...	
4209	93291	52 Leo	gG4	0.91	5.48	...	...	M *	5793 S 1	< 1.6	...	< -5.1	...	...	
4216	93497	μ Vel	G5III+G2V	0.90	2.69	...	...	M *	4448 208 1	185.8	8.4	-4.2	...	...	
4246	94247	44 UMa	K3III	1.36	5.10	1.1	0.016	S *	416 S 1	< 2.5	...	< -5.1	< 29.1	< 19	1
4301	95689	α UMa	K0IIIa	1.07	1.79	-0.3	0.038	M *	850 0 1	< 2.3	...	< -6.4	< 28.3	2.6	2
...	96161	62401	G5III	...	6.96	...	...	S	5208 S 2	< 10	...	< -3.7	...	...	
4436	100055	.....	G9III	0.93	6.56	...	...	S	6120 S 1	< 2.6	...	< -4.5	...	...	
4521	102328	.....	K3III	1.27	5.27	...	...	S *	6101 S 1	1.5	0.4	-5.2	...	< 19	1

TABLE 2—*Continued*

HR	HD	Name[a]	Spectral Type	B-V	m_v	M_v	Parallax (")	Flag[b]	Journal of Observations[c]	f_x[d] (10^{-13} erg cm^{-2} s^{-1})	Δf_x[d]	log f_x/f_v	log L_x	v sin$i$ ($km\ s^{-1}$)	Ref.
4527	102509	93 Leo	A7V+G5III-IVe	0.55	4.53	1.2	0.022	R *	5190 222 1	58.6	3.6	-3.9	30.2	< 50	1
4623	105452	α Crv	F2III-IV	0.32	4.02	3.2	0.070	M *	5538 0 1	17.4	2.4	-4.7	28.6	16	1
4637	105920	.....	G6III+a:	0.82	6.23	...	...	S *	5900 S 1	< 7.5	...	< -4.1	...	...	
...	106365	62904	K2III	1.13	6.88	...	...	M	3922 S 1	< 4.3	...	< -4.1	...	...	
4665	106677	.....	K0III	1.14	6.29	...	...	R *	3208 54 1	153.5	6.8	-2.8	...	...	
4666	106690	2 CVn	M1III+F7V	1.55	5.66	...	...	M *	4606 S 1	< 1.8	...	< -5.0	...	...	
4668	106760	.....	K0.5IIIb	1.14	5.00	1.7	0.022	M *	3922 S 1	< 4.1	...	< -4.9	< 29.0	< 17	1
...	107341	62953	K1III	1.00	6.73	...	...	M	5153 S 1	< 2.4	...	< -4.4	...	...	
...	107415	100054	K0III	1.04	6.47	...	...	S	4300 S 1	< 8.9	...	< -4.0	...	...	
4793	109519	.....	K1III	1.22	5.85	...	...	S *	3240 S 1	< 2.1	...	< -4.8	...	...	
4801	109742	25 Com	K5III	1.41	5.68	...	...	S *	1849 S 1	< 5.9	...	< -4.5	...	...	
4883	111812	31 Com	G0IIIp	0.67	4.94	0.1	0.011	S *	3917 S 1	59.8	4.1	-3.7	30.8	77	1
...	112278	100337	M4III	1.53	6.92	...	...	M	4037 S 1	< 2	...	< -4.4	...	...	
4924	112989	37 Com	G9IIICH-2Fe1Ca1	1.17	4.90	0.9	0.016	M *	10109 626 1	6.7	2	-4.7	29.5	10.4	5
4932	113226	ϵ Vir	G8IIIab	0.94	2.83	1.0	0.043	S *	7864 381 1	7.4	1.1	-5.5	28.7	2.7	5
4953	113994	.....	G7III	0.99	6.14	...	...	M *	6683 S 1	< 5.7	...	< -4.3	...	...	
4986	114780	.....	M0III	1.51	5.77	...	...	S *	3555 S 1	< 3.1	...	< -4.7	...	...	
5020	115659	γ Hya	G8IIIa	0.92	3.00	0.2	0.027	S *	7682 341 1	9.2	1.6	-5.3	29.2	< 17	1
5047	116365	65 Vir	K3III	1.43	5.89	...	...	S *	9703 S 1	< 1.6	...	< -4.9	...	...	
5078	117267	.....	K0III	1.11	6.43	...	...	S	144 S 1	< 8.3	...	< -4.0	...	...	
5102	117876	.....	G8III	0.96	6.11	...	...	M *	3212 S 1	< 6.9	...	< -4.2	...	...	
5104	118010	.....	K2III	1.26	6.44	...	...	S	1902 S 1	< 2.2	...	< -4.6	...	...	
5117	118319	.....	K0III	1.03	6.50	...	...	S	1902 S 1	< 2.5	...	< -4.5	...	...	
5130	118666	.....	F3III-IV	0.39	5.79	...	...	S *	7257 S 1	< 4.8	...	< -4.5	...	...	
5145	119081	.....	K3III	1.28	6.23	...	...	M *	6442 S 1	< 2.4	...	< -4.6	...	...	
5199	120499	.....	M6IIIe	...	7.40	...	...	M	3935 S 1	< 2	...	< -4.2	...	...	
5225	121107	7 Boo	G5III	0.84	5.70	...	...	S *	5377 S 1	7.1	1.3	-4.4	...	...	
5331	124681	.....	M4IIIab	1.60	6.45	...	...	S	4550 S 1	< 2.4	...	< -4.5	...	...	
5340	124897	α Boo	K1IIIbCN-1	1.23	-0.04	-0.1	0.097	S *	4450 208 1	< 2.6	...	< -7.1	< 27.5	2.4	2
...	127093	83375	M1III	1.59	6.69	...	...	S	2605 S 1	< 1.8	...	< -4.6	...	...	
5442	128000	.....	gK5	1.50	5.76	...	...	S *	6124 S 1	< 1.3	...	< -5.1	...	...	
5487	129502	μ Vir	F2III	0.38	3.88	2.1	0.045	M *	5564 0 1	44.3	2.8	-4.3	29.4	54	1
5506	129989	ϵ Boo	K0II-III	0.97	2.70	-1.3	0.016	M *	5565 0 1	< 1.1	...	< -6.4	< 28.7	6.6	4
5563	131873	β UMi	K4IIIBa0.3	1.47	2.08	0.0	0.039	S *	5567 0 1	< 1.4	...	< -6.5	< 28.0	< 17	1
5584	132525	.....	M2III	1.60	5.93	...	...	S *	3269 S 1	< 2.2	...	< -4.8	...	...	
5601	133165	110 Vir	K0.5IIIbFe-0.5	1.04	4.40	1.4	0.025	S *	6687 S 1	< 2	...	< -5.4	< 28.6	< 17	1
5638	134320	46 Boo	gK2	1.24	5.67	...	...	M *	4616 S 1	< 7.5	...	< -4.4	...	...	
5673	135402	.....	gK2	1.20	6.20	...	...	S *	3216 S 1	< 1.4	...	< -4.9	...	...	
5681	135722	δ Boo	G8IIICN-1	0.95	3.47	0.9	0.030	M *	7683 341 1	< 1.2	...	< -6.0	< 28.2	< 19	1
5714	136726	11 UMi	K4III	1.37	5.02	0.9	0.015	S *	6891 S 2	< 1.2	...	< -5.4	< 28.8	< 17	1
5739	137471	τ^1 Ser	M1III	1.66	5.17	0.7	0.013	S *	10086 S 2	< 1.9	...	< -5.2	< 29.1	...	
...	137570	101556	M2III	1.64	6.89	...	...	S	792 S 1	< 2.2	...	< -4.4	...	...	
5763	138481	ν^1 Boo	K5III	1.59	5.02	1.5	0.020	S *	3089 S 1	< 1.8	...	< -5.2	< 28.7	< 17	1
5785	138852	.....	K0III-IV	0.96	5.79	-2.7	0.002	S *	7328 S 1	< 1.8	...	< -4.9	...	...	
5791	138936	.....	F0III	0.28	6.56	...	...	S	5708 S 1	< 1.2	...	< -4.8	...	71	1
5796	139087	.....	gK0	1.09	6.07	...	...	M *	810 S 1	< 2.5	...	< -4.7	...	...	
5802	139195	16 Ser	K0III:CN1Ba0.7Sr2	0.95	5.26	2.6	0.030	M *	8919 S 2	< 10.3	...	< -4.4	< 29.1	< 17	1

TABLE 2—*Continued*

HR	HD	Name[a]	Spectral Type	B-V	m_v	M_v	Parallax (")	Flag[b]	Journal of Observations[c]	f_z[d] (10^{-13} erg cm^{-2} s^{-1})	Δf_z[d]	log f_z/f_v	log L_z	v sin$i$ ($km\ s^{-1}$)	Ref.
...	139216	101641	M5IIb-IIIab	1.39	6.25	...	...	S *	814 S 2	< 4.1	...	< -4.4	...	...	
5828	139778	.....	gK1	1.07	5.87	...	...	S *	10549 S 2	< 2.2	...	< -4.8	...	...	
5841	140117	.....	K1III	1.09	6.45	...	...	S	2614 S 1	< 5	...	< -4.2	...	...	
5854	140573	α Ser	K2IIIbCN1Fe4143-1	1.17	2.65	1.3	0.053	M *	4419 0 1	< 1.3	...	< -6.3	< 27.7	2	5
5861	140815	.....	K0III	1.19	6.33	...	...	S	3174 S 1	< 2.3	...	< -4.6	...	...	
5889	141714	δ CrB	G3.5III-IVFe-1	0.80	4.63	0.4	0.014	S *	7609 288 1	47.5	2.3	-4.0	30.5	< 17	1
5924	142574	.....	M0III	1.59	5.44	2.2	0.023	S *	371 S 1	< 3.4	...	< -4.8	< 28.9	...	
5935	142889	.....	K0III	1.01	6.31	...	...	S	3839 S 1	< 4.5	...	< -4.3	...	...	
5947	143107	ϵ CrB	K2IIIab	1.23	4.15	1.1	0.024	M *	1799 S 2	< 2.5	...	< -5.4	< 28.7	< 17	1
5958	143454	.....	sdBe+gM3+Q	0.10	2.00	...	...	M *	3189 34 1	< 1.9	...	< -6.4	...	...	
6008	145001	κ Her	G8III	0.95	5.00	-3.5	0.002	M *	7610 288 1	14.7	1.2	-4.4	...	10	1
6009	145000	κ Her	K1III	1.14	6.25	-2.2	0.002	M *	7610 288 1	14.7	1.2	-3.8	...	< 25	1
6056	146051	δ Oph	M0.5III	1.58	2.74	0.4	0.034	M *	5581 0 1	< 1.5	...	< -6.2	< 28.2	...	
6057	146084	.....	K2III	1.15	6.31	...	...	S	4105 S 1	< 3.9	...	< -4.4	...	...	
6072	146686	γ^2 Nor	G8III	1.08	4.02	2.2	0.044	M *	5150 S 1	< 2.2	...	< -5.5	< 28.1	< 12	1
6130	148374	.....	G8III	0.96	5.67	...	...	M *	4417 S 2	1.3	0.4	-5.1	...	...	
6132	148387	η Dra	G8IIIab	0.91	2.74	1.3	0.051	M *	4417 0 2	< 1.7	...	< -6.2	< 27.9	2.2	2
6145	148760	.....	K1III	1.08	6.10	...	...	S *	857 S 1	< 2.1	...	< -4.7	...	...	
6148	148856	β Her	G7IIIa	0.94	2.77	-0.3	0.024	M *	5584 0 1	11.7	1.5	-5.3	29.4	3.4	2
6166	149447	.....	K6III	1.57	4.16	0.9	0.022	S *	3311 S 1	< 9.8	...	< -4.8	< 29.4	...	
...	151061	141344	M5III	1.79	6.90	...	...	S	10443 S 2	< 0.9	...	< -4.8	...	...	
6241	151680	ϵ Sco	K2.5III	1.15	2.29	-1.0	0.022	S *	854 0 1	< 2.5	...	< -6.2	< 28.8	...	
6271	152334	ζ^2 Sco	K4III	1.37	3.62	0.9	0.028	S *	3140 S 1	< 7.1	...	< -5.2	< 29.0	...	
...	152783	208221	M6IIIe	1.54	6.10	...	...	M *	919 S 1	< 3.5	...	< -4.5	...	...	
6299	153210	κ Oph	K2III	1.15	3.20	0.7	0.031	S *	7686 341 1	< 1	...	< -6.2	< 28.1	< 17	1
6300	153221	.....	G8-K0III+G	0.88	6.00	...	...	M *	1042 S 1	< 6.8	...	< -4.3	...	...	
6321	153727	29 Oph	K0III	1.38	6.26	...	...	S *	5945 S 1	< 2.6	...	< -4.6	...	...	
6348	154391	.....	K1III	1.00	6.13	...	...	S *	5688 S 6	< 0.6	...	< -5.2	...	...	
6363	154732	.....	K1III	1.09	6.09	...	...	M *	7667 S 1	< 3.1	...	< -4.6	...	...	
6474	157588	.....	gK1	1.10	6.19	...	...	M *	10253 S 1	< 2.1	...	< -4.7	...	...	
6517	158619	.....	K2III	1.19	6.44	...	...	S	3222 S 1	< 6.8	...	< -4.1	...	...	
...	159881	185573	K5III	1.90	6.84	...	...	S	2522 S 1	< 3.1	...	< -4.3	...	...	
6566	159966	27 Dra	K0III	1.08	5.05	1.6	0.020	M *	5606 S 2	< 2.2	...	< -5.1	< 28.8	< 17	1
6587	160748	.....	M1III	1.81	6.40	...	...	S	2551 S 1	< 2.6	...	< -4.5	...	...	
6607	161193	.....	gK0	1.05	5.99	...	...	S *	7174 S 1	< 4.8	...	< -4.4	...	...	
...	162319	122806	K4III	1.39	6.75	...	...	S	3899 S 2	< 3.5	...	< -4.3	...	...	
6648	162391	.....	G8III	1.13	5.84	...	...	S *	2535 S 1	< 4.2	...	< -4.5	...	...	
6705	164058	γ Dra	K5III	1.52	2.23	-0.8	0.025	M *	2251 1 1	< 2.1	...	< -6.3	< 28.6	3.5	5
6724	164584	7 Sgr	F3III	0.52	5.34	-0.4	0.007	M *	3124 S 1	< 2.5	...	< -5.0	...	36	1
6763	165524	.....	gK3	1.23	6.15	...	...	S *	10433 S 1	< 0.7	...	< -5.2	...	...	
6803	166479	.....	B9V+F7III	...	6.09	...	...	M *	9928 S 1	< 1.1	...	< -5.0	...	...	
6820	167193	.....	K4III	1.47	6.12	...	...	S *	10613 S 1	< 1.3	...	< -4.9	...	...	
6858	168415	.....	K4III	1.47	5.39	...	...	S *	4582 S 1	< 2.1	...	< -5.0	...	...	
6869	168723	η Ser	K2IIIabCN1	0.94	3.26	2.1	0.058	S *	5616 0 1	< 1.2	...	< -6.1	< 27.6	2.5	6
6882	169110	.....	M0IIIab	1.60	5.41	...	...	S *	4910 S 1	< 1.1	...	< -5.3	...	...	
6935	170474	60 Ser	K0III	0.96	5.39	1.0	0.013	M *	2673 S 1	< 3.1	...	< -4.9	< 29.3	< 17	1
6940	170547	.....	G8II-III	0.95	6.28	...	...	M *	6578 S 1	< 1.3	...	< -4.9	...	...	

TABLE 2—*Continued*

HR	HD	Name[a]	Spectral Type	B-V	m_v	M_v	Parallax (")	Flag[b]	Journal of Observations[c]	f_x[d] (10^{-13} erg cm^{-2} s^{-1})	Δf_x[d]	log f_x/f_v	log L_x	v sin$i$ ($km\ s^{-1}$)	Ref.
6945	170693	42 Dra	K2III	1.19	4.82	1.4	0.021	M *	8820 S 2	< 2.8	...	< -5.1	< 28.9	< 17	1
6965	171237	25 Sgr	F3II-III	0.54	6.51	...	...	S	4971 S 1	< 1.5	...	< -4.7	...	17	1
6970	171391	.....	G8III	0.92	5.14	0.5	0.012	S *	1657 S 1	14.7	1.7	-4.3	30.1	< 19	1
6973	171443	α Sct	K3III-IIIb	1.33	3.85	-0.1	0.016	S *	7687 341 3	< 0.9	...	< -6.0	< 28.6	< 17	1
...	171911	31055	M4III-IIIb	1.58	6.67	...	...	S	927 S 1	< 1.1	...	< -4.8	...	...	
7007	172348	.....	gK4	1.55	5.84	...	...	M *	6581 S 1	< 1.7	...	< -4.9	...	...	
7020	172748	δ Sct	F2IIIpδDel	0.35	4.72	1.7	0.025	M *	8921 427 1	< 1.9	...	< -5.3	< 28.6	32	1
7024	172831	.....	K0-1III	1.00	6.15	...	...	M *	6586 S 1	< 2.6	...	< -4.6	...	...	
7117	174980	.....	K0II-III	0.92	5.27	1.8	0.020	S *	4066 S 1	< 3.1	...	< -4.9	< 29.0	< 17	1
7125	175306	o Dra	G9IIIbCN-0.5	1.19	4.66	-1.4	0.006	R *	4946 227 1	4.3	1.3	-5.0	...	20	1
7140	175635	.....	G8III+A2	0.91	6.02	...	...	M *	891 S 1	< 5.4	...	< -4.4	...	...	
7243	177940	.....	M7IIIev	1.60	6.09	...	...	M *	7451 3 1	< 1.8	...	< -4.8	...	...	
...	178637	104526	K1III	1.16	6.64	...	...	M	1273 S 1	< 1.3	...	< -4.7	...	...	
7310	180711	δ Dra	G9III	1.00	3.07	0.6	0.032	M *	5626 0 1	< 0.9	...	< -6.3	< 28.0	< 17	1
7321	181053	24 Aql	K0IIIa:Ba0.3CH1	1.05	6.41	1.4	0.010	M	10706 S 1	< 4.8	...	< -4.3	...	...	
7333	181391	26 Aql	G8III-IV	0.92	5.01	2.4	0.030	M *	8730 445 2	7.7	1.2	-4.6	29.0	< 17	1
7344	181645	ρ^2 Sgr	gG9	1.06	5.87	...	...	M *	8922 S 1	< 1.5	...	< -5.0	...	...	
...	182917	31632	M7IIIab+Be	1.69	7.08	...	...	M	4913 255 1	< 1.5	...	< -4.5	...	...	
7391	182955	.....	M0III	1.55	5.81	...	...	M *	8680 S 1	< 1.7	...	< -4.9	...	...	
7407	183492	.....	K0III	1.05	5.56	...	...	S *	1199 S 1	< 1.5	...	< -5.1	...	...	
7428	184398	.....	K2II-IIIe+A0V	1.16	6.37	...	...	R	3228 54 1	15.1	3.6	-3.8	...	< 50	1
7455	184996	.....	M0III	1.55	6.09	...	...	S *	7206 S 1	< 2.1	...	< -4.7	...	...	
7465	185264	.....	G9III	...	6.56	...	...	S	5632 S 1	< 2	...	< -4.6	...	...	
7472	185436	.....	K0III	0.96	6.48	...	...	S	5175 S 1	< 1.2	...	< -4.8	...	...	
7478	185734	ϕ Cyg	G8III-IV	0.97	4.69	-1.1	0.007	M *	3170 S 2	< 6.1	...	< -4.8	...	...	
7488	185958	β Sge	G8IIIaCN0.5	1.05	4.37	-0.4	0.011	S *	7821 S 3	< 2.1	...	< -5.4	< 29.3	8.9	4
...	187237	87733	G2III	0.63	6.88	...	...	S	1751 S 1	< 6.4	...	< -3.9	...	< 20	1
...	187614	87785	G8III	0.94	6.44	...	...	S	1751 S 1	6.4	1.7	-4.1	...	...	
7615	188947	η Cyg	K0III	1.02	3.89	-0.2	0.015	M *	3369 S 1	< 2.5	...	< -5.5	< 29.1	< 19	1
7663	190222	.....	K5III	1.58	6.45	...	...	S	3114 S 1	< 2.9	...	< -4.5	...	...	
...	190227	69307	K1III	1.20	6.42	...	...	S	5071 S 2	< 2.2	...	< -4.6	...	...	
...	192182	69597	G8III	1.10	7.10	...	...	M	827 S 1	< 0.9	...	< -4.7	...	...	
7795	194069	.....	G5III+A	1.07	6.39	...	...	S	5036 S 1	< 5.9	...	< -4.2	...	...	
7798	194152	.....	K0IIIv	1.08	5.58	...	...	M *	3482 S 1	5.5	1	-4.5	...	...	
7800	194193	.....	K7III	1.60	5.93	...	...	S *	5036 S 1	< 3.7	...	< -4.6	...	...	
...	194558	69986	K2/3III	1.27	6.74	...	...	M	779 S 1	< 2.3	...	< -4.4	...	...	
7867	196134	.....	K0III-IV	1.00	6.49	...	...	S	4221 S 2	< 1.6	...	< -4.7	...	...	
7884	196574	71 Aql	G8III	0.95	4.32	-0.7	0.010	M *	8415 S 3	1.1	0.3	-5.7	...	< 19	1
7942	197912	52 Cyg	K0III	1.05	4.22	0.1	0.015	M *	5273 S 3	< 5.1	...	< -5.1	< 29.4	< 17	1
7949	197989	ϵ Cyg	K0III	1.03	2.46	1.2	0.057	M *	4458 208 1	< 1.7	...	< -6.3	< 27.8	3	2
7956	198134	.....	K3III	1.32	4.92	-1.6	0.005	M *	4458 S 1	< 2.7	...	< -5.1	...	< 19	1
7964	198208	.....	K3III	1.42	6.21	...	...	M *	6271 S 1	< 2.9	...	< -4.5	...	...	
...	198624	50116	M3II-III	1.62	6.51	...	...	M	2182 S 1	< 2.4	...	< -4.5	...	...	
...	198626	70564	gF2	0.26	6.80	...	...	M	2206 S 3	< 6.7	...	< -4.0	...	...	
8005	199101	.....	gK5	1.52	5.47	...	...	S *	2184 S 1	< 2.3	...	< -4.9	...	...	
...	199547	50260	K0III	1.13	7.05	...	...	S	3821 S 1	< 3.1	...	< -4.2	...	...	
8035	199870	.....	K0IIIbCN-0.5	0.97	5.55	1.6	0.016	M *	3821 S 1	< 2.6	...	< -4.9	< 29.1	...	

TABLE 2—*Continued*

HR	HD	Name[a]	Spectral Type	B-V	m_v	M_v	Parallax (")	Flag[b]	Journal of Observations[c]	f_x[d] (10^{-13} erg cm^{-2} s^{-1})	Δf_x[d]	log f_x/f_v	log L_x	v sin$i$ ($km\ s^{-1}$)	Ref.
8080	200914	24 Cap	M0.5III	1.61	4.50	1.2	0.022	M *	3044 S 1	< 3.5	...	< -5.2	< 28.9	...	
...	201935	50547	F0III	0.35	6.63	...	...	S	4961 S 1	< 5	...	< -4.2	...	...	
8115	202109	ζ Cyg	G8III-IIIaBa0.6	0.99	3.20	0.4	0.027	M *	7868 381 1	< 0.9	...	< -6.3	< 28.2	3.4	4
8131	202447	α EQU	G0III+A5V	0.53	3.92	0.5	0.021	M *	5645 0 1	28.7	1.9	-4.5	29.9	< 50	1
8150	202987	.....	K3III	1.45	5.98	...	...	S *	8689 S 1	< 1.3	...	< -5.0	...	...	
8167	203387	ι Cap	G8III	0.9	4.28	1.9	0.033	S *	3536 99 1	63.8	4.8	-4.0	29.8	< 17	1
8168	203399	.....	K5III	1.5	5.95	...	...	S *	375 S 1	< 9.3	...	< -4.2	...	...	
8179	203574	.....	G5III	1.00	6.11	...	...	S *	6330 S 1	< 1.4	...	< -4.9	...	...	
8183	203638	33 Cap	K0III	1.16	5.41	2.0	0.021	S *	7797 S 1	< 4	...	< -4.7	< 29.0	...	
8191	203842	.....	F5III	0.47	6.35	...	...	S	10101 626 1	< 1.4	...	< -4.8	...	84	1
8207	204139	35 Cap	K5III	1.44	5.78	...	...	M *	7798 S 1	< 4.6	...	< -4.5	...	...	
8275	206040	.....	K1III	0.99	6.15	...	...	S *	8101 S 1	< 1.8	...	< -4.8	...	...	
8285	206356	41 Cap	G9III	0.95	5.24	2.2	0.025	M *	698 S 1	< 3	...	< -4.9	< 28.8	...	
...	209791	19826	F3III/IV	0.54	6.44	3.9	0.031	M	4899 179 1	7.8	2.8	-4.0	29.0	< 25	1
...	209813	51628	K0III+F1V	1.08	6.77	...	...	R	3230 54 1	84.2	8.1	-2.9	...	...	
8421	209857	.....	M4IIIab	1.61	6.13	...	...	S *	3230 S 1	< 4.7	...	< -4.4	...	...	
8448	210334	.....	G2IV+K0III	0.72	6.11	...	...	R *	5012 265 6	343.6	2.8	-2.5	...	...	
8449	210354	π^1 Peg	gG6	1.00	5.58	-0.5	0.006	M *	9029 S 1	< 1.6	...	< -5.1	...	...	
8453	210434	.....	K0III-IV	0.98	6.01	...	...	M *	7612 288 1	3.5	1	-4.5	...	...	
8454	210459	π^2 Peg	F5III	0.46	4.29	-1.5	0.007	S *	9029 480 1	< 3.1	...	< -5.3	...	120	1
8511	211833	25 Cep	K3III	1.26	5.75	...	...	S *	5949 S 2	< 5.2	...	< -4.5	...	...	
8575	213389	.....	K2III	1.15	6.40	...	...	R	3231 54 1	36.3	3.9	-3.4	...	...	
8594	213930	.....	G8III-IV	0.96	5.71	...	...	M *	1319 S 1	11.3	1.6	-4.2	...	...	
8654	215359	.....	K5III+K2III	1.48	5.95	1.0	0.010	M *	2681 S 1	< 5.1	...	< -4.4	...	...	
8684	216131	μ Peg	G8III	0.93	3.48	1.5	0.040	S *	7681 341 1	< 1	...	< -6.1	< 27.9	7	1
8703	216489	.....	K1-2II-IIIe	1.12	5.64	...	...	R *	3233 54 1	162.6	7.1	-3	...	...	
8775	217906	β Peg	M2.5II-III	1.67	2.42	-0.9	0.022	M *	858 0 1	< 1.9	...	< -6.2	< 28.7	...	
8789	218240	86 Aqr	G9III	0.90	4.47	1.7	0.028	M *	4293 S 1	< 3	...	< -5.2	< 28.7	...	
8828	219023	.....	G8-K0III	0.92	6.80	...	...	M	5159 S 1	< 1	...	< -4.8	...	...	
8886	220130	.....	K2III	1.61	6.39	...	...	M	6935 S 1	< 2.6	...	< -4.5	...	...	
8905	220657	υ Peg	F8III	0.61	4.40	2.2	0.036	S *	8396 449 2	41.1	1.9	-4.1	29.6	79	1
8961	222107	λ And	G8III-IV	1.01	3.82	2.3	0.050	R *	3235 54 1	603.3	14.6	-3.2	30.5	< 19	1
...	222390	91410	K1III	1.06	6.66	...	...	S	8356 S 1	< 1.5	...	< -4.6	...	...	
8979	222493	.....	G9III	1.00	5.89	...	...	M *	1915 S 1	< 1.5	...	< -5.0	...	...	
8987	222643	.....	K4III	1.37	5.28	1.2	0.015	M *	2294 S 1	< 3.5	...	< -4.9	< 29.3	< 17	1
8992	222800	.....	M7IIIpev	1.58	6.36	...	...	M	2294 S 1	< 2.5	...	< -4.6	...	...	
9015	223346	.....	F5III-IV	0.44	6.46	...	...	M	5667 S 1	< 1.8	...	< -4.7	...	12	1
...	223617	128417	G9IIIBa2	1.16	6.91	...	...	S	5667 S 1	< 2.1	...	< -4.4	...	...	
9030	223637	80 Peg	M3IIIa	1.66	5.79	...	...	S *	5744 S 1	< 0.9	...	< -5.2	...	...	
			Supergiants (luminosity classes II, I-II, and I)												
157	3421	.....	G2.5IIa	0.88	5.48	...	...	S *	4939 227 1	< 2.3	...	< -5.0	...	4	4
215	4502	ζ And	K1IIe	1.12	4.06	1.9	0.037	R *	3534 99 2	120.6	3.7	-3.8	30.0	40	1
...	13686	12195	K2.5Ib-II	1.87	7.01	...	...	S	7564 S 3	< 1.8	...	< -4.4	...	...	
...	17346	23632	G9II	1.26	6.82	...	...	S	5041 S 1	< 1.2	...	< -4.7	...	...	
...	25056	24350	G0Ib/II	1.20	7.03	...	...	S	5919 S 1	< 1.6	...	< -4.5	...	...	
1577	31398	ι Aur	K3II	1.53	2.69	-0.7	0.021	S *	2248 1 1	< 3.2	...	< -5.9	< 28.9	3.5	4

TABLE 2—*Continued*

HR	HD	Name[a]	Spectral Type	B-V	m_v	M_v	Parallax (")	Flag[b]	Journal of Observations[c]			f_z[d] (10^{-13} erg cm^{-2} s^{-1})	Δf_z[d]	log f_z/f_v	log L_z	v sin$i$ (km s^{-1})	Ref.
1603	31910	β Cam	G0Ib	0.92	4.03	-1.2	0.009	M *	4229	1	1	8.6	2	-5.0	...	19	1
1829	36079	β Lep	G5II	0.82	2.84	-0.7	0.020	M *	4416	0	1	3.4	0.8	-5.8	29.0	5.1	2
1922	37350	β Dor	F6Ia	0.82	3.76	-0.8	0.012	M *	9025	501	1	< 2.7	...	< -5.6	< 29.4	...	
2061	39801	α Ori	M1-2Ia-Iab	1.85	0.50	-6.0	0.005	M *	856	0	1	< 1.2	...	< -7.2	...	...	
2190	42475	.....	M0-1Iab	2.25	6.56	...	...	S	8373	398	1	< 1.5	...	< -4.7	...	...	
2197	42543	6 Gem	M1-2Ia-Iab	2.24	6.39	-1.2	0.003	S	5928	S	1	< 4.5	...	< -4.3	...	...	
2269	44033	.....	K3Ib	1.61	5.69	...	...	S *	5305	S	1	< 5.7	...	< -4.5	...	...	
2326	45348	α Car	F0II	0.15	-0.72	-3.5	0.028	S *	6960	0	2	45.6	1.4	-6.1	29.8	...	
2473	48329	ϵ Gem	G8Ib	1.40	2.98	-0.9	0.017	M *	4446	208	1	< 2.2	...	< -6.0	< 29.0	< 17	1
2580	50877	o^1 CMa	K2Iab	1.73	3.87	-4.6	0.002	S *	7872	S	3	< 1.8	...	< -5.7	...	< 19	1
2638	52622	.....	F2II	0.39	6.45	...	...	S	9961	S	1	< 10.5	...	< -3.9	...	...	
2646	52877	σ CMa	K7Ib	1.73	3.47	0.4	0.024	M *	5276	254	1	< 1.4	...	< -6.0	< 28.5	...	
2650	52973	ζ Gem	F7-G3Ib	0.79	3.79	...	...	M *	10643	501	2	< 1.2	...	< -5.9	...	< 54	1
2803	57623	δ Vol	F6II	0.79	3.98	-3.0	0.004	S *	7871	381	1	< 1.5	...	< -5.7	...	...	
...	59693	134775	F8Ibe	1.18	5.82	-2.7	0.002	S *	4943	227	1	< 2.8	...	< -4.7	...	...	
2993	62576	1 Pup	K3Ib	1.63	4.59	0.9	0.018	M *	3872	S	2	< 1.2	...	< -5.6	< 28.6	...	
3045	63700	ξ Pup	G3Ib	1.24	3.34	-4.3	0.003	M *	7866	381	1	< 1.1	...	< -6.1	...	...	
3102	65228	11 Pup	F7II	0.72	4.20	1.0	0.023	S *	8722	S	1	< 4.1	...	< -5.2	< 29.0	21	1
3185	67523	ρ Pup	F6IIpδDel	0.43	2.81	0.5	0.035	M *	8916	427	1	5.6	1.5	-5.6	28.7	14	1
...	73502	220186	G1Ib	0.69	6.42	...	...	S	734	S	1	< 5.4	...	< -4.2	...	...	
3445	74180	.....	F3Ia	0.71	3.84	1.3	0.031	M *	742	S	1	< 6.3	...	< -5.2	< 28.9	38	1
3459	74395	.....	G1Ib	0.84	4.62	-1.2	0.007	M *	7867	381	1	< 1.2	...	< -5.6	...	< 17	1
3496	75276	.....	F2Iab	0.56	5.75	...	...	S *	736	S	1	< 12.5	...	< -4.1	...	...	
4159	91942	.....	K3-4II	1.62	4.45	1.5	0.026	M *	3339	S	1	< 2.2	...	< -5.4	< 28.6	...	
...	95950	251235	M2Ib	2.04	6.75	...	...	S	2161	1	1	< 2.4	...	< -4.4	...	...	
4522	102350	.....	G5Ib-II	0.90	4.11	-0.7	0.011	M *	3943	S	1	< 4.2	...	< -5.2	< 29.6	...	
4786	109379	β Crv	G5II	0.89	2.65	0.3	0.034	S *	4449	208	1	< 4.6	...	< -5.8	< 28.7	3.8	2
...	114988	63419	G2II	0.78	6.67	...	...	M	5205	S	1	< 4.2	...	< -4.2	...	...	
...	117000	252326	F2Ia	1.08	6.62	...	...	S	7469	S	1	< 1.5	...	< -4.7	...	...	
...	126009	83312	M3II	1.60	6.66	...	...	S	5557	S	1	< 1.3	...	< -4.7	...	...	
6498	157999	σ Oph	K2II	1.50	4.34	-1.1	0.008	S *	4230	1	1	< 1.4	...	< -5.6	...	3.2	4
6536	159181	β Dra	G2Ib-IIa	0.98	2.79	-1.6	0.013	M *	3812	128	1	26.5	3.1	-5.0	30.3	13	1
6615	161471	ι^1 Sco	F2Iae	0.51	3.03	-0.6	0.019	M *	4080	S	1	< 2.5	...	< -5.9	< 28.9	36	1
6695	163770	θ Her	K1IIaCN+2	1.35	3.86	-4.6	0.002	S *	2250	1	1	< 2.1	...	< -5.6	...	3.4	4
6742	164975	γ^1 Sgr	F4-G1Ib	0.78	4.69	...	...	M *	2532	S	2	< 4.1	...	< -5.0	...	25	1
7032	173009	ϵ Sct	G8II	1.12	4.90	0.9	0.016	M *	6582	S	1	< 1.4	...	< -5.4	< 28.8	6.5	4
7475	185622	.....	K4Ib	2.07	6.38	...	...	M	5275	S	1	< 1.6	...	< -4.7	...	...	
7525	186791	γ Aql	K3II	1.52	2.72	-1.3	0.016	S *	7688	341	1	< 0.8	...	< -6.5	< 28.6	3.2	4
7570	187929	η Aql	F6Ibv	0.89	3.90	-1.1	0.010	M *	4444	208	1	< 2	...	< -5.6	...	...	
7741	192713	22 Vul	G3Ib-II	1.04	5.15	-1.8	0.004	M *	2679	S	1	< 2.1	...	< -5.1	...	17	1
...	193469	69820	K5Ib	1.90	6.30	...	...	M	7875	S	1	< 2.1	...	< -4.7	...	...	
7796	194093	γ Cyg	F8Ib	0.68	2.20	-5.4	0.003	M *	779	S	1	< 2.3	...	< -6.3	...	20	1
7932	197572	.....	F7Ib-G8Ibv	1.23	6.47	...	...	M	6812	S	1	< 1.9	...	< -4.6	...	22	1
7988	198726	.....	F5Ib	0.72	5.77	-0.3	0.006	M *	3793	S	1	< 4.3	...	< -4.6	...	...	
...	200102	50333	G1Ib	1.05	6.62	...	...	S	3054	S	1	< 4.9	...	< -4.2	...	...	
8079	200905	ξ Cyg	K4-5Ib-II	1.65	3.72	-2.1	0.007	M *	3813	128	1	< 1.3	...	< -5.9	...	< 17	1
8126	202314	.....	G6Ib-IIaCa1Ba0.3	1.09	6.17	...	...	S *	7868	S	1	< 1.7	...	< -4.8	...	...	

TABLE 2—*Continued*

HR	HD	Name[a]	Spectral Type	B-V	m_v	M_v	Parallax (")	Flag[b]	Journal of Observations[c]			f_x[d] (10^{-13} erg cm^{-2} s^{-1})	Δf_x[d]	log f_x/f_v	log L_x	v sin$i$ (km s^{-1})	Ref.
8204	204075	ζ Cap	G4Ib	1.00	3.74	...	...	M	* 5648	0	1	< 1.3	...	< -5.9	...	< 19	1
8232	204867	β Aqr	G0Ib	0.83	2.91	-3.2	0.006	M	* 4441	208	1	< 2	...	< -6.0	...	18	1
8308	206778	ϵ Peg	K2Ib	1.53	2.39	-3.7	0.006	M	* 4443	208	1	< 1.8	...	< -6.3	...	< 17	1
8313	206859	9 Peg	G5Ib	1.17	4.34	-1.1	0.008	S	* 4445	208	5	< 1.8	...	< -5.5	...	20	1
8321	207089	12 Peg	K0IbHδ0.5	1.41	5.29	-0.8	0.006	S	* 3814	128	1	< 1.5	...	< -5.2	...	...	
8571	213306	δ Cep	F5Ib-G2Ib	0.60	3.75	-1.0	0.011	M	* 9024	501	1	< 1.3	...	< -5.9	< 29.1	9	1
8796	218356	56 Peg	G8Ib	1.34	4.76	-1.3	0.006	M	* 4233	1	1	22.4	2	-4.2	...	< 17	1
9053	224165	.....	G8Ib	1.16	6.00	...	...	S	* 4618	S	1	< 2.3	...	< -4.7	...	...	

[a] A single number (five or six digits) in the "Name" column is from the Smithsonian Astrophysical Observatory (SAO) catalog.

[b] We classify a source (or upper limit) to be single (S) or multiple (M) according to the criteria explained in § II*c*. The "R" symbol is used to indicate RS CVn–like systems. An asterisk flags the stars with $m_v < 6.3$.

[c] The three numbers in this column represent the IPC sequence number, the observer code in the *Einstein* observing catalog (see below), and the total number of observations for each star. In the case of multiple observations we quote, for conciseness, only the sequence with the longest live time. Observer code: (S) serendipitous CfA stellar survey; (0) Harvard-Smithsonian Center for Astrophysics X-ray stellar team; (1) Columbia Astrophysical Laboratory; (2) MIT; (3) Goddard Space Flight Center; (34) J. Nelson and F. Cordova, University of California, Berkeley; (54) C. Bowyer, F. Walter, and P. Charles, University of California, Berkeley; (97) R. Stern, J. Underwood, and S. Antiochos, Jet Propulsion Laboratory; (99) C. Zwaan, A. Brinkman, and R. Mewe, Sonnenborgh Observatory; (128) T. Ayres, B. Haisch, and J. Linsky, University of Colorado; (179) T. Snow, and W. Cash, University of Colorado; (208) J. Linsky, and T. Ayres, University of Colorado; (222) C. Bowyer, and F. Walter, University of California, Berkeley; (227) H. Zirin, Hale Observatory; (254) J. Linsky, R. Stencel, and G. Basri, University of Colorado; (255) G. Wallerstein, and L. Willson, University of Washington; (265) D. Gibson, New Mexico Tech; (288) S. Catalano, C. Blanco, E. Marilli, G. Peres, and S. Serio, University of Catania; (322 H. Johnson, Lockheed Research Laboratory; (341) B. Haisch, and T. Simon, Lockheed Research Laboratory; (381) L. Hartmann, and A. Dupree, Harvard College Observatory; (385) C. Zwann, A. Boggende, A. Brinkman, and R. Mewe, Sonnenborgh Observatory; (398) A. Michalitsianos, M. Kafatos, and R. Hobbs, Goddard Space Flight Center; (427) G. Riegler, R. Stern, and J. Underwood, Jet Propulsion Laboratory; (445) C. Bowyer, F. Walter, and F. Charles, University of California, Berkeley; (449) T. Simon, R. Stencel, M. Giampapa, and J. Linsky, University of Colorado; (480) C. Bowyer, B. Bopp, and F. Walter, University of California, Berkeley; (501) E. Böhm-Vitense, and S. Parson, University of Washington; (519) R. Stern, I. Underwood, and S. Antiochos, Jet Propulsion Laboratory; (544) C. Zwaan, and R. Mewe, Sonnenborgh Observatory; (572) D. Heeschen, C. Casini, and J. Heidmann, National Radio Astronomy Observatory-VA; (626) T. Simon, and R. Stencel, University of Colorado; (994) H. Johnson, Lockheed Research Laboratory.

[d] X-ray fluxes at Earth, and statistical errors. See § III*d* for details on the case of multiple observations.

REFERENCES.—(1) Hoffleit and Jashek 1982. (2) Gray 1982. (3) Herbig and Spalding 1955. (4) Gray and Toner 1986. (5) Gray and Nagar 1985.

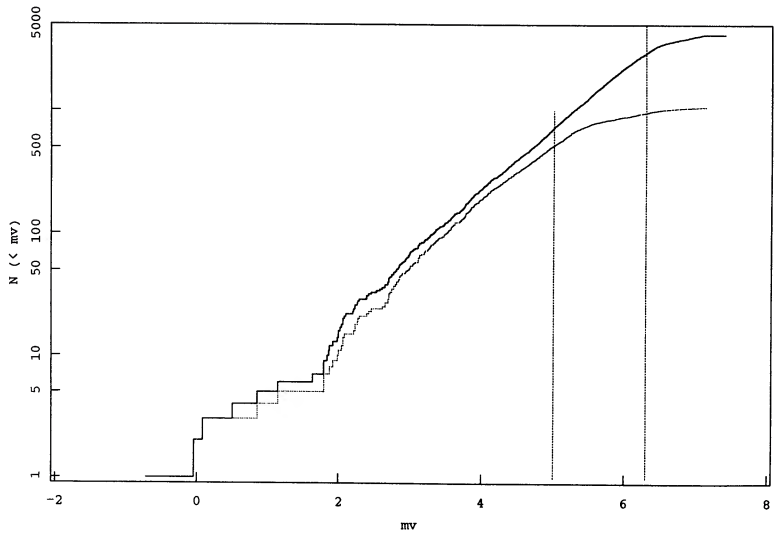

FIG. 1.—Integral distribution functions of the apparent visual magnitude, m_v, for giant and supergiant stars in *The Bright Star Catalogue*. Solid line refers to the total sample, while dotted line is for stars having measured parallaxes and within 100 pc. Two vertical lines at $m_v = 6.3$ and $m_v = 5$ indicate, respectively, the thresholds at which the total sample and the distance-limited sample can be considered complete.

sample with available trigonometric parallax and distance $D < 100$ pc (about 32% of the giants and 31% of the supergiants meet this condition). The vertical bars on top of the figure show the $B-V$ color distribution of all the other stars with unknown distance or unreliable parallax (216 giants and 42 supergiants). To get a hint about the range of masses explored and about the evolutionary stage of the stars in our survey, we have superposed on Figure 2 four theoretical evolutionary tracks: the lowest three tracks (0.7, 1.1, and 2.2 $M_\odot$) have been computed by Sweigart and Gross (1978) and Mengel *et al.* (1979), assuming initial abundances $Y = 0.3$ and $Z = 0.01$, and the 3 $M_\odot$ track has been adopted from Becker (1981), where $Y = 0.28$ and $Z = 0.01$ are assumed. For the transformation of the theoretical H-R diagram to the color-magnitude diagram, we have used the complete $T_{\rm eff}:B-V:$BC scales of Flower (1977). Some comments are in order about the appearance in this diagram of a series of clusterings and gaps:

1. The minor clustering around $B-V \sim 0.4$ is due mainly to F giants or subgiants which are just evolving off the main sequence, but have not yet entered the Hertzsprung gap. We stress in this context that, in spite of their MK classification, the "giant" F stars (luminosity classes III–IV, III, II–III) in the BSC nearer than 100 pc (a total of 81 stars) have a mean absolute visual magnitude of $\langle M_v \rangle = 2.4$, more compatible with class IV–V stars (Allen 1973); that is, the BSC F giants appear to be almost exclusively low-luminosity stars, therefore implicitly low-mass stars (1–2 $M_\odot$), in the slow evolutionary phases preceding the run across the Hertzsprung gap. The F giants in our survey mimic the composition of the optical parent sample; we warn the reader not to interpret the results about the X-ray emission of the F giants (§ IV*a*) as appropriate to stars more massive than $\sim 2\ M_\odot$.

2. The crowded region at $B-V \sim 1$ is populated by the numerous late G and early K giants located at the base of the ascending red giant branch. The evolutionary models (Iben 1967; Becker 1981) indicate that stars of 3 $M_\odot$ or more cross this region for the first time when they leave the Hertzsprung gap moving to the right, and cross a second time evolving in the opposite direction and more slowly, during the He burning phase. Because of the different evolutionary time scale at the two epochs, Alschuler (1975) conjectured that G5 III and earlier stars are first crossing (FC) objects of intermediate mass and age, whereas G8 III to late K III stars are mostly second crossing (SC) objects. We note, however, that most stars in our sample limited to $D < 100$ pc appear to have $M \lesssim 3\ M_\odot$, according to the adopted evolutionary tracks.

3. Finally, the clustering around $B-V \sim 1.6$ is mainly an artifact of using the $B-V$ color scale (instead of, e.g., the $V-R$ color, not available in the BSC), which is not a reliable indicator of the effective temperature for stars later than spectral type K 8 III: $B-V = 1.6$ is in fact a threshold value of this color index for giant stars, while $T_{\rm eff}$ keeps decreasing beyond this point (Johnson 1966; Flower 1977).

In order to extend the results about the X-ray properties of our observed sample to the larger optical sample, it is important to check whether the observed sample is representative of the optical parent population from which it has been drawn. For this reason, we have compared the cumulative distribution functions of three interesting parameters in both samples: namely, the $B-V$ color, the absolute visual magnitude M_v, and the distance D. To make the comparison more easily interpretable, we have considered five subsamples, one for each spectral type among the giants and one more comprising all supergiants. It is worth noting that $\sim 26\%$ of the observed giant stars are targets of pointed observations; this percentage rises to $\sim 52\%$ for the supergiant sample. Hence, the danger of observational bias is very strong, especially in the latter case. We have computed cumulative distribution functions of the three parameters $B-V$, M_v, and D for the five optical subsamples described above, and for the corresponding observed subsamples. For reasons of completeness explained before, we have used all stars with $m_v < 6.3$ to build the $B-V$ distributions, while only the stars with $m_v < 5$ and $D < 100$ pc have been selected for the other distributions. We have applied nonparametric two-sample tests (Schmitt 1985) in order to compare each pair of distributions ("optical" vs. "observed" distributions), where the null hypothesis is that they are statistically indistinguishable. These tests show that in none of the

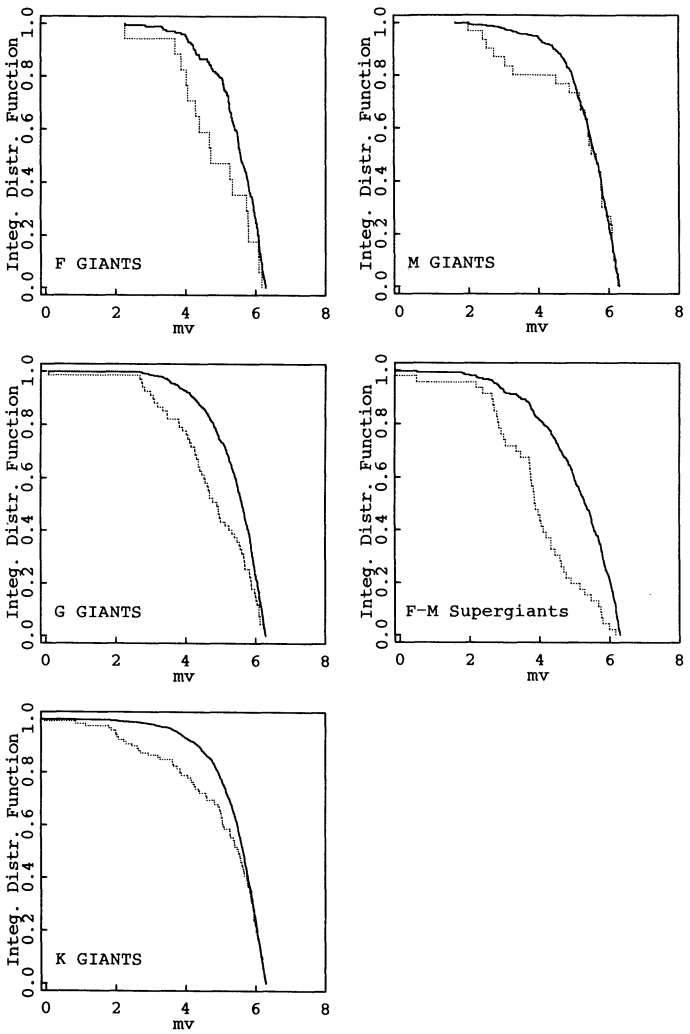

FIG. 2.—H-R diagram for the X-ray observed sample. Plus symbols indicate giant stars, asterisks refer to bright giant and supergiant stars, while RS CVn–like systems are represented by the symbol "R." Vertical bars on top of the diagram show the $B-V$ color distribution of stars with no trigonometric parallax available or with distance greater than 100 pc. Solid lines are evolutionary tracks for stars with the indicated masses (see text for references and more details).

cases we can reject the null hypothesis at the 99% confidence level, with the sole exception of the M_v distributions for the K giants; the difference at the 99.6% level between the optical and the X-ray sample is due to the null sampling of $\sim 10\%$ of the stars in the optical sample with low absolute luminosity ($M_v \gtrsim 2$). In other words, for each considered spectral class, the optical and observed subsamples could have been drawn from the same parent population, with the only possible exception of the K giants.

To clarify this finding better, we have also compared the distributions of the apparent visual magnitude m_v for the optical sample and the observed sample, including all stars with $m_v < 6.3$ (see Fig. 3): we have found that the distributions for the G giants and for the F–M supergiants are indeed statistically different, at the 99% level, while for the K giants there is a marginal difference at the 98.5% level. A similar result could be inferred for the F giants, but the statistics is poorer. We interpret this difference as a result of an oversampling of nearby and apparently more luminous stars introduced by the pointed observations. We do not see this effect when comparing the distance distributions, because we are missing most of the faraway and faintest stars which do not have available or reliable parallaxes. However, we also note that the low-luminosity tails (high m_v) are increasingly more populated going from the F to the M giants, as a result of an increasing number of serendipitous observations. In fact, in a magnitude-limited sample, the faintest objects tend to be intrinsically bright stars at large distances, and we know that the absolute visual luminosity is greater for redder stars. Hence, a large number of these stars are present in the optical sample and likely fall in the *Einstein Observatory* fields of view. We conclude that while the pointed observations give preference to nearby objects, the serendipitous observations recover most of the faintest (but intrinsically bright) and distant stars. The final selection effect is probably only a nonuniform space coverage of the survey objects, and in particular an undersampling of stars at intermediate distances; the lack of most parallaxes prevents a more rigorous proof of this statement. This bias is of no importance if the distribution of the absolute visual magnitude is the same for the optical and the observed sample. Again, we must restrict ourselves to the smaller sample of stars with $D < 100$ pc, and we have already seen that only the K giants may represent a potential problem. However, unless the X-ray emission is proved to depend strongly on M_v, the lack of $\sim 10\%$ of low visual luminosity K giants will not affect the conclusions drawn from the analysis of the X-ray data.

In summary, our observed sample is representative of the optical parent population as far as the spectral type distribution is concerned. The large number of serendipitous observations, especially for the giant stars, also prevents any strong bias regarding the visual luminosity distribution; only the nearby observed K giants are proved to be incomplete at the low-luminosity tail.

c) *Multiple Systems and RS CVn–Type Stars*

Like previous studies, we want to emphasize the need for careful discrimination between single stars and multicomponent systems. In the latter case, we expect to generally observe an enhancement in the level of radiation for two reasons: (i) in principle, all components may contribute as independent emitters to the total observed luminosity; (ii) in the case of close systems, the orbital motion may induce fast surface rotational velocities by means of tidal coupling, and hence increase the nonthermal heating of the individual stellar chromospheres and coronae, if provided by a magnetic dynamo mechanism. This second effect is probably at work in the RS CVn systems (Walter and Bowyer 1981; Pallavicini *et al.* 1981; Majer *et al.* 1985), which may also be affected by a physical interaction between the surface magnetic field structures of the system components (Walter, Gibson, and Basri 1983).

For these reasons, we have decided to flag the stars in our sample with any of the following indications of multiplicity as reported in the BSC: (*a*) confirmed or suspected spectroscopic binaries (88 objects), (*b*) stars with either a physical or visual companion nearer than 2′ (56 objects), because of the photon collecting area we used (see § III), (*c*) stars with variable radial velocity, unless a companion is known at more than 2′ (32 objects), (*d*) 10 more objects with three or more components for which we cannot judge the distance of the nearest companion. We may conjecture that the absence of any indication of binarity is due to lack of close observations: to test this hypothe-

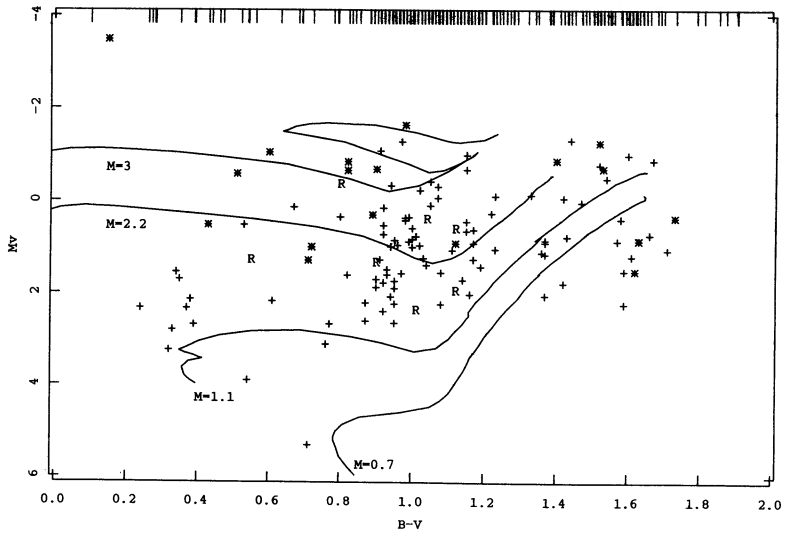

FIG. 3.—Integral distribution functions of the apparent visual magnitude, m_v, for the optical parent sample (*solid line*), and the X-ray observed sample (*dotted line*), for the indicated spectral types. Only stars with $m_v < 6.3$ are included. Nonparametric two-sample tests show that for the G giants and for the F–M supergiants, the X-ray sample distribution is statistically distinguishable from the optical sample distribution, at the 99% confidence level.

sis, we compared the distance distributions of single stars versus multiple stars as defined above, but we found that these two distributions are not statistically distinguishable, with a high degree of certainty.

We have also searched for the occurrence of known RS CVn systems (including both short-period and long-period systems) in our list of observed stars, using as a reference the list of Strassmeier *et al.* (1988). We found 16 such systems in the observed sample and have treated them separately. However, we feel that other stars in our sample may belong to this class, but have not been recognized as such, because no detailed study of their nature has been carried out. In this respect, we notice that the RS CVn systems in our sample (see R symbols in Fig. 2) cannot be distinguished from the bulk of G and K giants among which they are scattered, judging solely on their position in the H-R diagram. We have found that six RS CVn systems (two of them without reliable distances, hence not displayed in Fig. 2) fall in the region $1 < B-V \leq 1.12$: because of so many RS CVn's in the region where the TRDL is believed to occur, their behavior as X-ray emitters is extremely important in the context of our study.

III. THE X-RAY DATA

a) X-Ray Sources

The X-ray data were obtained with the *Einstein Observatory* imaging proportional counter (IPC) (Giacconi *et al.* 1979; Gorenstein, Harnden, and Fabricant 1981). For this survey, we have employed the final REV-1 data processing (Harden *et al.* 1984) in a fashion well tested in previous works (Maggio *et al.* 1987; Micela *et al.* 1988). We have now organized all relevant X-ray data into a stellar data base (Sciortino *et al.* 1988; Harnden *et al.* 1989) which readily allows us to perform extensive analyses on the 429 IPC images comprising our survey (see the journal of observations in Table 2).

The standard REV-1 source detection algorithm analyses each image with two different detection methods: the "local" method, which searches for fluctuations with respect to the local background, and the "map" method, which differs in that it uses a reference map to determine background. The first method finds fewer spurious detections in regions with diffuse or intense emission, but the second method is more sensitive, especially in fields crowded with weak sources. Both methods are applied in three energy bands: soft (0.2–0.8 keV), hard (0.8–3.5 keV), and broad (0.2–3.5 keV). A detection cell of 2.4 × 2.4, for the broad and hard bands, and 4′ × 4′ for the soft, is moved across the image to find possible sources by comparison to standard detection thresholds (expressed in terms of a minimum signal-to-noise ratio). The thresholds are chosen so that no more than 0.3 spurious detections can be expected, on average, for each method and each band in any field. In order to reduce the probability of spurious detections, we adopted an approach more restrictive than that used by REV-1 system; namely, we retained only broad-band detections (from either the local or the map method—five detections failed this criterion). For the same reason, we have discarded detections with a signal-to-noise ratio less than 0.6 above the detection threshold; this conservative choice (which eliminated 10 detections) reduces the statistically expected number of spurious detections to 0.01 per field.

In our survey, X-ray sources were identified by matching the positions of all optical candidates with the positions of X-ray detections present in the ~4000 IPC exposures. Our matching criterion stipulates that a given star has been observed and detected if it is located within 2′ of the position of any X-ray detection (in fact, only two sources fall at more than 1′ from the corresponding optical candidate). With the above criteria, we have found 84 X-ray sources corresponding to 69 different stars which are distributed among the various spectral types as illustrated in Table 1.

b) X-Ray Upper Bounds

As a result of the standard IPC processing, upper limits to the X-ray fluxes are available for all objects listed in the *Einstein Observatory* master catalog, which includes some 60 different catalogs (Harris and Irwin 1984). Most stellar entries come about due to the inclusion of the SAO catalog, the Kukarkin catalog, and the Two-Micron Sky Survey catalog. We have derived X-ray 3 σ upper bounds for all members of

our optical sample that fall within 2′ of the position of an object from the master catalog. The total number of such sample stars is 313, observed in 375 fields, with about 14% of the stars having been observed more than once. Only three multiply-observed stars failed to be detected in each repeated exposure: for these three stars, the derived upper limits are consistent with the X-ray fluxes derived from the detections.

c) *Spurious Sources*

As explained above (see § III*a*), the number of expected spurious sources (statistical background fluctuations) is 0.01 per field, which translates into 4.29 spurious sources in 429 unique fields. Since 460 objects (with repetitions) have been observed, the probability that one of them falls in a detection cell taken at random is

$$p = \frac{\text{(object area)(total number of objects)}}{\text{(cell size)(number of cells per field)(number unique fields)}} = 3.7 \times 10^{-3},$$

where we have assumed that the area covered by each object is that of a circle with radius of 2′, the cell size is 2.′4 × 2.′4, and the total field size is 1 deg^2. This is also the probability that any of the spurious sources occur at the position of one of our survey stars; hence, the mean number of spurious identifications is

$$n_s = \text{(spurious sources per field)(number unique fields)}p = 1.6 \times 10^{-2}.$$

We have also estimated the probability of chance coincidence of one of our survey stars with either a main-sequence field star or an extragalactic source. The expected number of detectable field stars in our survey has been computed using the best current (summer 1987) estimates of the X-ray luminosity functions for each spectral type of the nearby dwarf stars. The procedure takes into account the actual sky distribution of the survey fields and the mean limiting sensitivity of each field, as extensively described in Favata *et al.* (1988) and Micela *et al.* (1988) and predicts a total of ~95 field stars in our total survey area. In a similar way, we have used the Medium Sensitivity Survey results of Maccacaro *et al.* (1982) to compute the expected number of extragalactic sources, finding that 276 such objects could be detected in our combined IPC exposures. We expect, therefore, a total of 371 objects in the combined fields of view and, in fact, we have detected 384 sources, in addition to the 84 sources identified with survey stars. Assuming that the 371 unrelated sources are scattered uniformly over the field of view, like the spurious detections, the quantity p is again the probability of one mistaken identification; hence, we see that $n_f = 371 \times p = 1.4$ field objects could have been spuriously identified with stars in our survey. We stress that the likelihood of such mistaken identification is much greater than for the case of background fluctuations.

d) *Source Strength*

In computing an effective count rate for each source, the standard REV-1 processing applies corrections, for mirror scattering and vignetting and for the IPC point response, and flags possible shadowing by the support structure of the IPC entrance aperture through the use of a so-called rib and edge code. However, due to a spectral dependence of these corrections (in particular, the point response correction), they are only approximate for sources whose spectra are dissimilar to those assumed in computing the corrections. Because the detection cell for the broad band is relatively small for the rather soft stellar sources, only ~70% of stellar source counts fall inside the cell, a fraction about 25% smaller than assumed in computing the standard correction factors. Therefore, for local, obscured X-ray detections, and for all map detections, we have increased the standard (corrected) values by this factor of ~25%, and for all local, unobscured X-ray detections we have computed net source counts from a circle of 3′ radius centered at the source position and background counts in a concentric annulus with inner and outer radii of 5′ and 6′. This same 25% correction has been applied to the upper bounds (which are only evaluated using the local method). When more than one observation was available for a given star, we adopted the following procedure (see Micela *et al.* 1988 for additional details):

1. For detections, we computed a weighted (by inverse square of statistical error) mean count rate, preferring unobscured measurements to those for which shadowing was possible.

2. For upper bounds, we selected the lowest unobscured value, if available, and otherwise conservatively retained the largest value.

In order to convert IPC count rates to X-ray fluxes at Earth in the energy range 0.16–4.0 keV, we have used a constant conversion factor of 2.0×10^{-11} ergs count^{-1} cm^{-2}. This value assumes a thermal spectrum (continuum + lines), from a plasma with solar abundances at a temperature log $T = 6.5$. Schmitt *et al.* (1988), using the thermal model of Raymond and Smith (1977), have performed spectral fits on the 29 sample sources that yielded more than 50 total counts, and we have compared the X-ray fluxes derived using the constant conversion factor with those derived from the spectral fits, finding good agreement (within a scatter of $\lesssim$40%). Schmitt *et al.* (1988) have also verified that in most cases good fits can be obtained neglecting the circumstellar or interstellar absorption of the X-ray radiation. The only two exceptions are HR 8703 (RS CVn–type system), and HR 8796 (56 Peg), for which the best fit is obtained with hydrogen column densities of 8×10^{19} and 2.5×10^{20} cm^{-2}, respectively. Incorporating this absorption yields an increase of the flux by 14%, and 35% for these two stars.

The final X-ray fluxes (along with their statistical uncertainties), and the 3 σ upper limits for all survey stars are listed in Table 2. Taking into account a conversion factor error of ~50%, statistical errors of $\lesssim$40%, and systematic errors in the instrument calibrations of $\lesssim$10%, we estimate the overall error in the quoted X-ray fluxes to be $\lesssim$70%.

In the computation of luminosities, a large source of error can be introduced by uncertainties in the individual stellar distances (as much as a factor of 2 or more); for this reason, we have computed X-ray luminosities only for stars with available trigonometric parallaxes greater than 0.01. Finally, in Table 2 we have also listed the values of the $\log f_x/f_v$, the logarithm of the X-ray to visual flux ratio, computed as

$$\log f_x/f_v = \log f_x + m_v/2.5 + 5.47 .$$

This distance- and radius-independent parameter is very useful in our survey because of the large percentage of stars with unknown parallax.

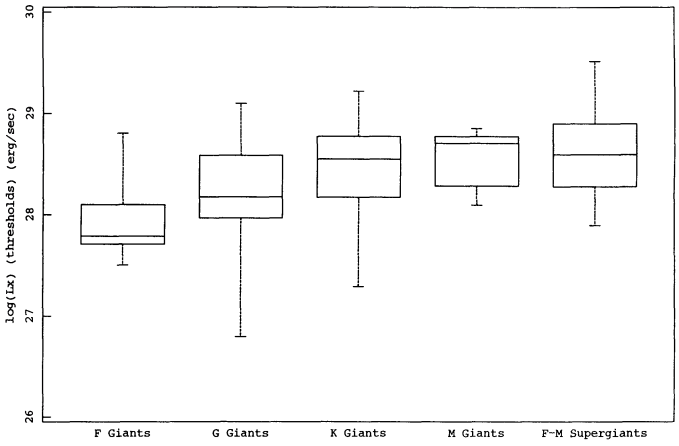

FIG. 4.—Schematic distribution of the X-ray luminosity thresholds for observations of survey stars within 100 pc. For each indicated spectral type, the horizontal line drawn through the box is at the median of the data, upper and lower edges of each box indicate the range of values including the middle half of the data, and vertical lines ("whiskers") reach the most extreme values. Note the increase in the median values (decrease in the sensitivity) for advancing spectral type.

e) X-Ray Sensitivity of the Survey

Because of the magnitude-limited nature of our survey, and the dependence of the absolute visual luminosity both on stellar color and on luminosity class, stars of different spectral types have necessarily been sampled, on average, at different space depths. For example, the intrinsically brighter M giants have been observed at larger distances with respect to the F giants. Except for pointed observations, which comprise only a small fraction of our fields, observing times were not chosen to sample stellar luminosities uniformly; indeed, even the mean X-ray flux sensitivity, f_z^t, which is fixed by the available exposure time and by the mean background count rate, varies greatly and independently of the spectral class of the observed star. Hence, the resulting X-ray luminosity thresholds, L_x^t, are, on average, larger for the visually brighter and more distant stars (e.g., for M giants or supergiants as compared to other giants). For those stars with measured parallax, the actual values of L_x^t can be computed; their distributions for different spectral types, shown schematically in Figure 4, confirm the expected behavior. Hence, the X-ray luminosity functions we will introduce below are not comparable in a straightforward manner because of the differences in luminosity thresholds. In § V, we discuss useful techniques for circumventing this problem.

We note that the pointed observations of nearby stars are very valuable, since they usually yield the highest sensitivities and allow us to sample the low X-ray luminosity tails of the distributions. In the case of the K and M giants, we were not able to sample above the median values of L_x or f_x/f_v (see § IV), but some high-sensitivity observations were exploited to put very low upper limits on the X-ray emission level of these star samples.

IV. RESULTS

We have detected X-ray emission from 62 giants and seven supergiants, distributed among the various spectral types as shown in Table 1. In the following, we will analyse the luminosity functions of the star classes which we have effectively sampled, with the aim to study the dependence of X-ray emission on spectral type and the effects of stellar evolution on such emission. For reasons of completeness (see § II*a*), we have computed the f_x/f_v distribution functions using all stars with $m_v < 6.3$, while the L_x distributions are based only on the stars with $m_v < 5$, and distance within 100 pc.

In order to derive the statistical properties of the data at hand, we have used survival analysis techniques which allow us to take into account both measurements and upper limits. In particular, we have computed maximum-likelihood distribution functions using the Kaplan-Maier product limit estimator described by Schmitt (1985) and Feigelson and Nelson (1985), and we have performed comparisons of sample distributions by means of nonparametric two-sample tests in the presence of censored data, as discussed by the same authors. In Table 3, we

TABLE 3

MEAN AND MEDIAN VALUES[a] ON $\log f_x/f_v$ AND $\log L_x$ (0.2–4 keV)

SPECTRAL TYPE	$\log f_x/f_v$					$\log L_x$				
	D[b]	U[b]	Mean	Median	Probability[c]	D[b]	U[b]	Mean	Median	Probability[c]
Giant Stars: Full Sample										
F	8	9	$-5.1^{+0.2}_{-0.2}$	$-5.1^{+0.1}_{-0.7}$		7	1	$28.7^{+0.2}_{-0.1}$	$28.57^{+0.06}_{-0.05}$	
G	30	37	$-5.3^{+0.1}_{-0.1}$	$-5.5^{+0.1}_{-0.3}$		15	15	$28.6^{+0.3}_{-0.4}$	$28.4^{+1.0}_{-1.4}$	
K	17	101	...	<-6.6	100%	6	30	...	<27.6	100%
M	1	29	...	<-6.2	94%	1	4	...	<28.9	94%
Giant Stars: Single Star Sample										
F	3	3	$-4.9^{+0.2}_{-0.2}$	$-5.0^{+0.2}_{-0.3}$		3	0	$28.9^{+0.4}_{-0.2}$	$28.7^{+0.9}_{-0.2}$	
G	10	14	$-5.3^{+0.2}_{-0.2}$	$-5.5^{+0.1}_{-0.6}$		7	6	$28.7^{+0.4}_{-0.4}$	$28.7^{+1.1}_{-1.7}$	
K	2	51	...	<-6.2	94%	1	13	...	<28.1	94%
M	0	16	...	<-5.3	94%	0	0		No stars	
Bright Giant and Supergiant Stars: Full Sample										
F–M ...	7	39	...	<-6.3	94%	5	14	...	<28.6	94%

[a] For purpose of computing mean and median values, we have used (i) stars with $m_v < 6.3$, for the $\log f_x/f_v$ distributions, (ii) stars with $D < 100$ pc and $m_v < 5$, for the $\log L_x$ distributions.

[b] Number of detections (D) and upper limits (U) which satisfy the criteria described in note (a).

[c] Probability associated with the estimated upper limits on median values (see § IV).

summarize mean and median values which have been derived from the integral distribution functions discussed below. The 68% (1 σ) errors are computed using a bootstrap technique (Schmitt 1985) with 200 replications. We recall that the integral distribution functions so obtained can be formally normalized only when no upper limit occurs below the lowest detection value. In some cases (K and M giants, F–M supergiants), our survey observations have been unsuccessful in detecting most of the stars sampled with the greatest sensitivity. In these cases, the integral distribution functions do not reach the median value, because this value probably lies near the lowest detection thresholds, or even below. Although no X-ray mean or median values can be obtained, we can derive upper bounds to the X-ray medians for these samples. If we are sampling with detection thresholds below the median luminosity, we should detect at least one-half (within statistics) of the objects sampled. Hence, the probability of sampling n times below the median and obtaining only upper limits is at most $(0.5)^n$. Following this reasoning, the fourth most sensitive upper limit is an $\sim$94% confidence upper bound to the median value of the distribution. If the fourth most sensitive observation resulted in a detection, we quote that value as a 100% upper limit on the median.

a) F Giants

We have detected 47% of all the observed F giants with $m_v < 6.3$, and this percentage does not change even if we consider only the single stars (six observed and three detected). In Figure 5*a*, we show the integral distribution functions of the f_x/f_v for the complete sample and the subsample of the single F giants. These distributions appear to be quite similar, suggesting that the X-ray emission of the multicomponent systems is not enhanced with respect to the emission of the single giant stars. In fact, we have compared the f_x/f_v distribution functions of single and multiple sources by applying a two-sample Wilcoxon rank test, and we have found that these two samples are drawn from the same parent population with a probability of $\sim$50%. In Figure 5*b*, we compare the X-ray luminosity functions of all stars ($m_v < 5$, $D < 100$ pc) regardless of multiplicity with the distribution of the single stars only. As in the previous case, these distributions are not statistically distinguishable.

The star with the lowest X-ray emission is β Cas (HR 21, log $f_x/f_v = -5.8$, log $L_x = 28.2$), a spectroscopic binary which is also a δ Sct variable. This star is the nearest F giant observed ($D = 14$ pc), and is also the star with the highest visual luminosity ($M_v = 1.6$). On the other extreme, the star with the highest X-ray luminosity is ν Peg (HR 8905, log $L_x = 29.6$, log $f_x/f_v = -4.2$), a single late-F giant which belongs to the Hyades moving group. Most of the nondetected stars lack trigonometric parallaxes; however, the star with the lowest upper limit on both the X-ray luminosity and the f_x/f_v ratio is the prototype of the dwarf Cepheids, δ Sct (HR 7020, $D = 40$ pc), with log $L_x <$ 28.6 and log $f_x/f_v < -5.4$. These values are compatible with the X-ray emission level of β Cas. We note in passing that we have observed two more stars classified as δ Sct variables: ρ Pup (HR 3185, F6 IIp) has been detected with log $L_x = 28.7$, log $f_x/f_v = -5.7$, while for HR 4668 (K0.5 IIIb) we have derived log $L_x < 29.0$, and log $f_x/f_v < -4.9$. An unpublished *Einstein* survey of six other δ Sct variables failed to detect other objects of this class (Stern 1988, private communication).

In summary, the observed F giant stars show X-ray emission in the narrow range of luminosity $10^{28} < L_x \lesssim 4 \times 10^{29}$ ergs s^{-1}, similar to the range spanned by the main-sequence F stars (see § V*b*). The corresponding range of the f_x/f_v ratio goes from 1.6×10^{-6} to 10^{-4}, and no distinction can be made between the single F giants and those which are part of multicomponent systems. The two observed early-type dwarf Cepheids show the lowest emission level among all the F giants in this survey.

b) G Giants

The success rate of detecting G giant stars was $\sim$45% if we consider the whole sample with $m_v < 6.3$, or $\sim$42% by taking into account the single stars only. As before, we compare in Figures 5*a* and 5*b* the integral distribution functions for the total sample and the single star sample, using in turn log f_x/f_v and log L_x as parameters of the X-ray emission level. Again, we find that no statistically significant distinction is possible, at the 90% level, between the two subsamples of single and multiple G giants. This result is quite surprising, since six RS CVn systems are included in the multiple star sample. In fact, we find that these systems have X-ray luminosities in the range[2] $30.2 <$ log $L_x < 31.3$, but the X-ray luminosities of two single G giants also fall in this range: they are 31 Com (HR 4883) with log $L_x = 30.8$ and δ CrB (HR 5889) with log $L_x = 30.5$. The former star has the bluest color ($B-V = 0.67$) among the G giants without a blended spectrum, and it is probably crossing the Hertzsprung gap, as suggested by its location in the H-R diagram and by the high abundance of lithium (Alschuler 1975; Hoffleit and Jashek 1982; Simon 1984). No similar information is available for δ CrB. Two more single G giants with a high emission level are worth mentioning: HR 6970 (G8 III, $B-V = 0.92$, $m_v = 5.14$) with log $L_x = 30.1$, and ι Cap (HR 8167, $B-V = 0.90$) with log $L_x = 29.8$. These stars are to be compared with μ Peg (HR 8684) and ϵ And (HR 163), two nearby ($D < 30$ pc) single G giants with similar $B-V$ color and identical spectral type, but low X-ray emission: log $L_x <$ 27.9 and log $L_x < 28.1$, respectively. This behavior is a characteristic common to the late G and early K giants: the stars with color $B-V \sim 1$ show the largest range in X-ray emission among all the giants in our survey, from the high-luminosity level of the RS CVn systems ($L_x \gtrsim 10^{30}$ ergs^{-1}) to the low upper limits on L_x of μ Peg and η Cap (HR 6132, G8 IIIab, suspected spectroscopic binary with a dK2 companion, log $L_x < 27.9$). The X-ray source with the reddest color is o Dra (HR 7125, $B-V = 1.19$), an RS CVn–type system with the lowest emission level among the detected stars of this class (log $f_x/f_v = -5.0$, log $L_x = 30.1$ uncertain because $D > 100$ pc). The reddest single G giant detected is 40 Psc (HR 1563) at $B-V = 0.98$ (log $f_x/f_v = -4.6$, no distance available). Finally, we note that we have failed to detect most of the G stars nearer than 30 pc (four detections, eight upper limits), but these high-sensitivity observations allow us to put strong constraints on the X-ray emission of many G8 III–G9 III stars: for example, HR 1008, the nearest G giant observed ($D = 6.2$ pc), has an upper limit on the X-ray luminosity of log $L_x < 27$, which is more than one order of magnitude below the emission level of the weakest G giants detected (log $L_x \sim 28.4$).

In conclusion, the G giants show a wide range of X-ray luminosities, and this is likely not the result of either stellar multiplicity or the uncertainty in distance determination. Some

[2] Here we have considered only the four stars with distances less than 100 pc: HR 373, HR 8961, HR 1708, and HR 4527, in order of decreasing L_x. Note that HR 373 (log $L_x = 31.3$) was not included in the sample used to built the luminosity function of the G giants because it has $m_v > 5$.

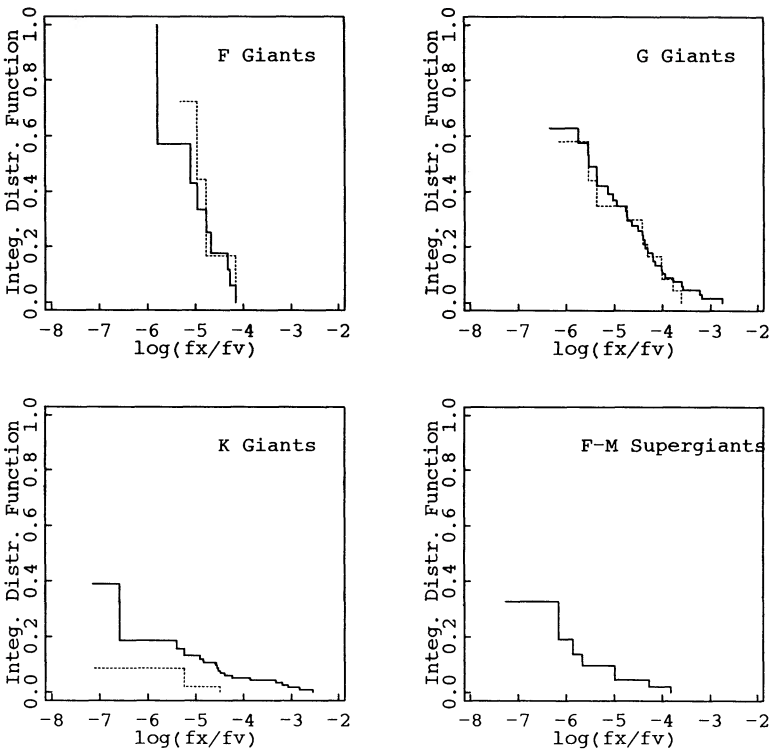

FIG. 5*a*

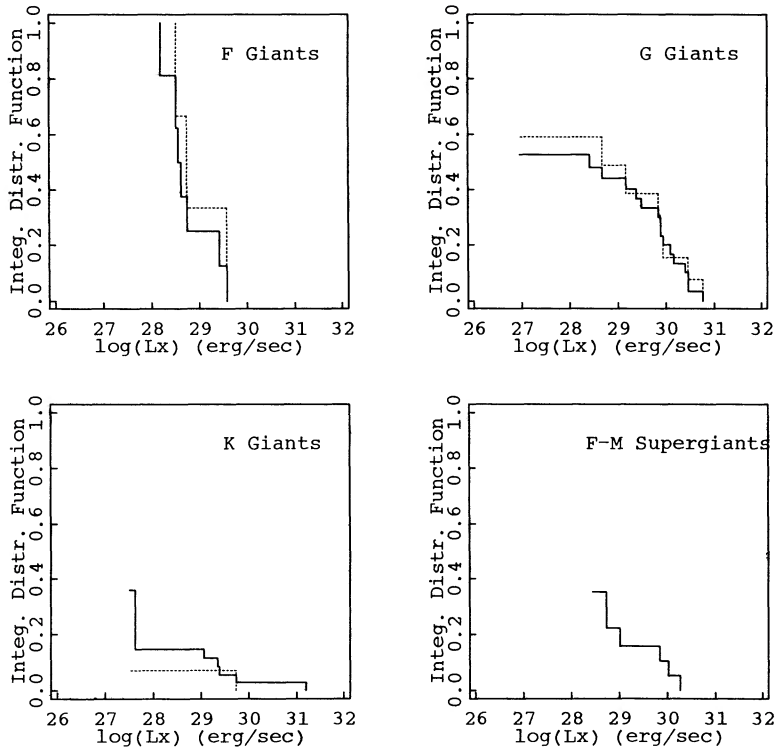

FIG. 5*b*

FIG. 5.—(*a*) Integral distribution functions of the X-ray to visual flux ratio, f_x/f_v, for stars of the indicated spectral types, with $m_v < 6.3$; (*b*) Integral X-ray luminosity functions for stars with $m_v < 5$ and $D < 100$ pc. For the giants, solid lines refer to all stars regardless of multiplicity, dotted lines to nonbinary stars only; note the high X-ray luminosity tails for the G and K giants (only one single K giant within 100 pc and $m_v < 5$ has been detected). For the supergiants, only global distributions are shown, regardless of spectral type or multiplicity, because of the small sample size; note, in particular, that only one single supergiant (α Car, F0 I) has been detected. In all cases, the lowest value reached by the curves indicates either the lowest detection (if the curve is normalized to 1; see F giants) or otherwise the lowest upper limit.

single G giants have a level of emission comparable to that of known RS CVn systems, but we have also observed stars where no X-ray emission has been detected at a sensitivity of $\sim 10^{28}$ ergs s^{-1}, a value typical of old G dwarf stars. Similar conclusions can be drawn from inspection of the f_x/f_v ratios, which span the range from $\sim 2.5 \times 10^{-4}$ down to $\lesssim 7 \times 10^{-7}$, where only single stars have been considered.

c) K Giants

We were able to detect only $\sim 14\%$ of the K optical candidates ($m_v < 6.3$). Moreover, most of the X-ray sources are multicomponent systems (15 out of 17 detections). For these reasons, we were able to compute only the high-luminosity tails of the log L_x and f_x/f_v distributions, as shown in Figure 5. If we compare the f_x/f_v distributions for the single star sample versus the sample of all the other stars, we find that these two samples are drawn from the same parent population with a probability of $\sim 0.5\%$; hence, the null hypothesis can be rejected at the 99% confidence level (however, this confidence level may be somewhat inaccurate, because the single star sample is limited and heavily censored). By comparing the X-ray luminosity functions (single vs. multiple stars, within 100 pc and $m_v < 5$), we find a lower significance level (probability of being drawn from the same distribution is $\sim 26\%$), probably because most of the RS CVn systems with a giant K component lack trigonometric parallaxes, and hence are not included in the sample used to build the L_x distributions. Instead, these objects form the high-luminosity tail of the f_x/f_v integral distribution for the whole sample. In fact, the eight K giants with the highest f_x/f_v ratio ($\log f_x/f_v \gtrsim -3.8$) are all RS CVn systems.

We have studied more in detail the six K sources within 100 pc. One of them is β Cet (HR 188), a nearby ($D = 16.4$) single K0 III star with a fairly high X-ray luminosity ($\log L_x = 29.7$, $\log f_x/f_v = -4.5$). Three others are γ, δ, and τ^1 Tau, the Hyades K0 giants. Although these are all spectroscopic binaries, the X-ray emission (again quite high, $\log L_x \gtrsim 29$) probably originates from the K0 III primaries, and not from a companion. This has been strongly argued by Baliunas, Hartmann, and Dupree (1983) on the basis of UV data analysis, and by Micela *et al.* (1988), who have presented the *Einstein Observatory* X-ray survey of the Hyades region. One more detected K giant is β Gem, a multicomponent system with a K0 giant as primary star and seven more optical companions: the brightest of them is more than 3′ from the primary, but unfortunately no more information is available in the BSC for the other components. At any rate, the X-ray luminosity of β Gem is lower ($\log L_x = 27.6$) with respect to the K0 giant sources mentioned above. The last star is σ Gem (HR 2973), an RS CVn–type system with a K1 III primary component and much higher luminosity ($\log L_x = 31.2$).

One more single K giant detected is HR 4521 ($\log f_x/f_v = -5.2$, no distance available), which is the reddest ($B-V = 1.27$) single star detected in our whole survey. This star has been recognized as a super metal-rich star by Faber *et al.* (1985). Among the nondetections we note α Boo (HR 5340, $D = 10.3$ pc), the nearest K star observed: for this single giant, we have obtained upper limits of $\log L_x < 27.5$ and $\log f_x/f_v < -7.1$, the lowest among the stars of this group (see also Ayres, Simon, and Linsky 1982). A low upper limit was also obtained for η Ser (HR 6869, $\log L_x < 27.6$, $\log f_x/f_v < -6.1$) which is the nearby ($D < 20$ pc) single K giant with the bluest color ($B-V = 0.94$).

We conclude that the single K giants are usually not detected as X-ray sources, with the exception of some K0 III stars whose behavior mimics the G giants. The RS CVn systems constitute about half of the stars detected and show $1.5 \times 10^{-4} \lesssim f_x/f_v \lesssim 2.5 \times 10^{-3}$. Other detected multicomponent systems have f_x/f_v as low as $10^{-6.6}$ and $L_x = 10^{27.6}$ ergs s^{-1} (β Gem, HR 2990, $D = 10.6$ pc). For the nearest K giants (seven stars within 20 pc, two detected), we were able to put upper limits of 10^{28} ergs s^{-1} on the X-ray luminosity, compatible with the emission level of the detected β Gem.

d) M Giants

Little can be said about the X-ray emission of the M giants because of the relatively high detection thresholds of the 30 observed stars with $m_v < 6.3$. Only one star has been detected: η Gem (HR 2216, $D = 71$ pc), a spectroscopic binary plus a third component of unknown spectral type. For this system, $\log L_x = 29.4$, and $\log f_x/f_v = -5.6$. Although we cannot determine whether the source is the M giant or one of its (lower mass, typically dwarf) companions, we note that either companion may contribute to the observed emission and still be consistent with known X-ray emission properties of such lower mass dwarf stars. The nearest M giant observed is δ Oph (HR 6056, $D = 29.4$), for which any X-ray emission, if present, is constrained by the upper limits, $\log L_x < 28.2$, $\log f_x/f_v < -6.2$.

In conclusion, the sensitivity of our survey of M giants does not go deep enough to allow to build up integral distribution functions. However, we can estimate upper bounds to the median values of log L_x and log f_x/f_v (Table 3), based on the fourth most sensitive upper limit criterion described in the opening of this section.

e) F–M Supergiants

We have detected seven supergiants out of 46 observed with $m_v < 6.3$; because of the small sample we will not separately analyse the four different spectral types. Nineteen stars have distances within 100 pc (five of them are detected), and only one source was identified with a single star (see below). Because of the similar absolute visual magnitude of the supergiants, all the spectral types have been sampled in the same volume of space. For all the above reasons, we have preferred to build global integral distribution functions of log L_x and log f_x/f_v, as shown in Figures 5*a* and 5*b*, regardless of multiplicity or spectral type.

Among the detections, α Car (HR 2326, $D = 36$ pc, $\log f_x/f_v = -6.2$, $\log L_x = 29.8$) stands alone in being the only single supergiant detected and the one with the bluest color ($B-V = 0.15$, F0 II). All the other X-ray sources are identified with multicomponent systems, and in none of these cases do we know the spectral classifications of the companions. One of these systems (ζ And, HR 215, $D = 27$ pc) is classified as an RS CVn–type binary, and its f_x/f_v ratio is the highest among the supergiants ($\log f_x/f_v = -3.8$, $\log L_x = 30.0$), but its X-ray luminosity is the lowest among the observed RS CVn's with known distance (except HR 3, which was not detected).

Because of the usually large distances, we are not able to put upper limits on the X-ray luminosities of the supergiants as stringent as for the giants. We have observed nine stars within 50 pc. Three have been detected: ζ And, α Car, and the δ Sct variable ρ Pup (see § IV*b*), while for the others we find upper limits of $L_x \lesssim 3$–8×10^{28} ergs s^{-1}. Among the nondetections, we also find four classical Cepheids (ζ Gem, δ Cep, η Aql, β Dor), and five so-called "hybrid" stars (Hartmann, Dupree,

and Raymond 1980) (γ Aql, β Aqr, ι Aur, τ Her, σ Oph). From the X-ray point of view, none of them is peculiar with respect to other supergiants of similar spectral type.

Our conclusions about the X-ray emission of the supergiants are based on a sample $\sim 20\%$ as large as that of the giants: this is due to the low space density and large distances of the former. Moreover, we should point out that all the observed supergiants within 100 pc have $M_v > -2$, except α Car ($M_v = -3.5$); hence, they are representative of a class of relatively low-mass objects. This is also true for the optical BSC population of late-type supergiants. α Car is the only observed (and detected) star of type F0; therefore, we cannot judge if X-ray emission is characteristically present in early F supergiants. The emission of all other X-ray sources may originate from any component of the observed systems. Finally, we put upper limits on the X-ray luminosity of most of the observed supergiants, which are somewhat higher than the level of giant stars of similar spectral type. In fact, we will show in the next section that our data are consistent with no strong dependence of L_x on the luminosity class.

V. DISCUSSION

a) The X-Ray Dividing Line

In § IV, we have noted how the percentage of detected giant stars decreases with advancing spectral type, with a remarkable drop at spectral type K. As a whole, we have detected too few supergiants to search for a similar trend. We now ask whether the low percentage of detected K and M giants is due to a selection effect; namely, the larger mean distance of these stars with respect to the F and G giants. To answer this question, we have intercompared the complete luminosity functions shown in Figure 5, using a Peto-Prentice generalized Wilcoxon test (Feigelson and Nelson 1985). This two-sample statistical test is the least affected by the detection threshold distributions of the compared samples. We have found that the X-ray luminosity function of the K giants is statistically different from those of the F and G giants at the 90% confidence level. We have derived a similar result for the $\log f_x/f_v$ distributions. To strengthen this conclusion, we have performed a further test: assuming that the true X-ray luminosity function of the K and M giants is identical to that of the G giants (Fig. 5*b*), we have computed the expected number of detectable K and M stars within 100 pc, given the actual X-ray luminosity thresholds of these samples. We have estimated that 22 K giants and three M giants should have been detected if the hypothesis is correct, while in fact we have detected six K giants and one M giant (see Table 3). The ratio of the predicted to the observed number of K stars is 3.7, and the 99% confidence level interval is [14.5,1.1], computed by assuming binomial statistics and the maximum likelihood procedure described by Gehrels (1986) for small samples. We therefore can exclude the possibility that the observed X-ray luminosity function for the K giants is the same as that for the G giants. Small sample statistics preclude such a strong conclusion for the M giants. Such results are unaffected by substituting the X-ray luminosity function of the F giants as a predictor. Thus, the drop of detections at spectral type K is a real effect, and not a consequence of the magnitude-limited nature of the observed star sample.

We have also tested the dependence of the X-ray emission level on the luminosity class by comparing the distributions of $\log L_x$ for giant and supergiant stars as a whole. We have derived a probability greater than 40% for the two samples being drawn from the same parent population, whether or not the RS CVn systems are included. Similar low significance results have been obtained by binning the stars according to the absolute visual magnitude instead of the luminosity class. The star sample with $M_v \leq 0$ (11 objects with $m_v < 5$, $D < 100$ pc), and the complementary sample with $M_v > 0$ (37 objects with $m_v < 5$, $D < 100$ pc) are drawn from the same parent population with a probability greater than 20%. The poor sampling of the supergiants in our survey does not allow us to explore in full detail a possible dependence of the X-ray emission drop on the luminosity class. Hence, we cannot prove (or even disprove) a possible bending of the X-ray dividing line to exclude the supergiant stars from the active star side.

b) Comparison with Main-Sequence Stars

In Figure 6, we show a comparison between the X-ray integral luminosity functions of giant stars and main-sequence stars with same spectral type. The dF stars ($0.3 \leq B-V \leq 0.5$) are from the work of Schmitt *et al.* (1985), the G dwarfs are those within 25 pc studied by Maggio *et al.* (1987), and the main-sequence K stars are from the survey of Bookbinder (1985). For this latter sample, we show in Figure 6*c* two luminosity functions corresponding to young disk and old disk stars, selected according to the kinematical criterion of Eggen (1969). The aim of the comparison with the giant stars under study is again to assess a possible dependence of the X-ray emission level on the luminosity class among the late-type stars. It is important to stress that stars with similar color but different luminosity class usually have different masses; therefore, we are comparing stars which do not follow the same evolutionary tracks. By using the Peto-Prentice generalized Wilcoxon test we have found that only the distribution functions of the G stars are distinguishable at the 90% confidence level, and the same holds for the K giants with respect to the young-disk K dwarfs. Since all RS CVn systems have been excluded from the dG sample while no such selection has been made for the G giants, we have performed a further comparison between the X-ray luminosity functions for the single G stars only, but the test outcome has not changed. The latter result is not unexpected, because we have already noted that presumed single G giants exist which are X-ray emitters at the same level of known RS CVn's. No such high-luminosity sources ($\log L_x > 29.5$) are present among the nearby G dwarfs. The mean X-ray luminosity for the G giants is about a factor 10 greater than for the nearby dG stars.

The median X-ray luminosity of the young-disk K dwarfs is more than a factor 4 greater than for the *K*-evolved stars. However, the high-luminosity tails for the two samples are similar (Fig. 6*c*). We have noted already that most of the detected K giants within 100 pc are binaries or multicomponent systems, but the X-ray emission of these few K sources is likely due to the K0 III primary component and not to a companion. In this respect, the K0 giants appear to be similar to the contiguous G giants, and we speculate that they represent the most advanced evolutionary phase of first-crossing stars, in which X-ray activity is still observed. If these high-luminosity K0 giants are excluded, the comparison with the K dwarfs clearly points out the lower X-ray emission level of the other red giants.

In conclusion, the X-ray luminosity of the observed F giants (most of them are slightly evolved low-mass stars) is comparable to that of the nearby dF stars, while the G giants are, on average, substantially brighter than main-sequence stars of

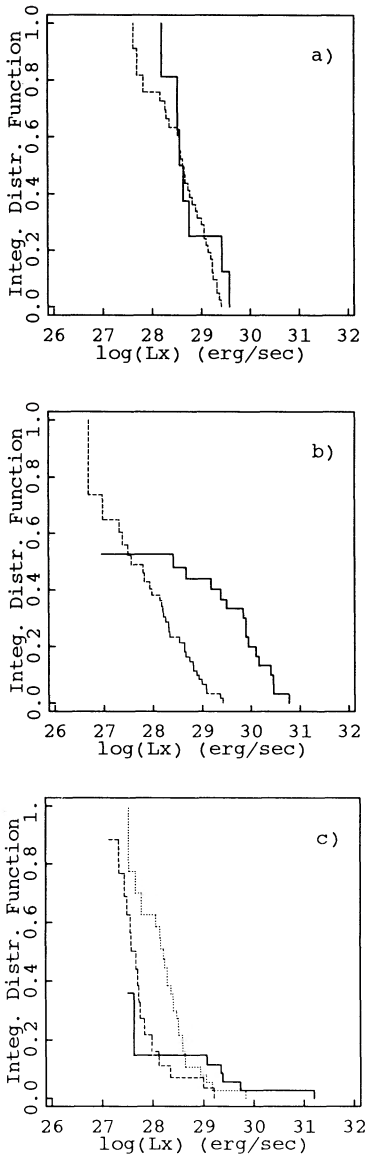

FIG. 6.—Comparison of X-ray luminosity functions for giants and main-sequence stars. (*a*) Giant F stars (*solid*) vs. F dwarfs, with $0.3 \leq B-V \leq 0.5$ (*dotted*), adapted from Schmitt *et al.* (1985); (*b*) giant G stars (*solid*) vs. F7–G9 dwarfs (*dotted*), adapted from Maggio *et al.* (1987); (*c*) giant K stars (*solid*) vs. old disk K dwarfs (*dashed*), and young disk K dwarfs (*dotted*), adapted from Bookbinder (1985). X-ray luminosity functions for the giant stars include all the objects with $m_v < 5$ and $D < 100$ pc. Note how the X-ray luminosity function for the G giants extends to much higher values than the corresponding distribution for main-sequence G stars.

similar spectral type, and the very early K giants show emission at the same level of corresponding young-disk dwarfs. We confirm the very modest emission level (if any) of the red giants with respect to the red dwarfs, as already suggested by the early studies of Vaiana *et al.* (1981), and Ayres *et al.* (1981).

c) *Onset of Magnetic Dynamo*

The plot in Figure 7 shows how the X-ray luminosity varies as a function of the $B-V$ color. To explore possible data trends, we have applied a robust locally weighted regression (Cleveland 1979), modified to take into account both detections and upper limits, to the sample of single stars only (*dotted line*). We observe a trend of increasing $\log L_z$ with $B-V$, up to the value $B-V \sim 0.8$ (late G type), followed by a drop for redder colors. A similar behavior has been noted by Simon (1984) for the normalized C IV flux (1549 Å), $f_{\rm C\,IV}/f_{\rm bol}$, and tentatively attributed to the amplification and the eventual decay of magnetic dynamo activity, as stars cross the Hertzsprung gap. Following the solar analogy, the EUV line emission probably originates in the transition region of the observed stars, and the similar behavior followed by the X-ray coronal emission does not come unexpected, although it should be confirmed on a more solid statistical ground. We note in Figure 7 a residual scatter about the mean trend in the X-ray emission level, which in part must surely be attributed to a mixture of stars with different masses at a fixed value of $B-V$. This is clearly shown in Figure 8, an H-R diagram in which each star is indicated by a circle with radius proportional to $\log L_x$ (*solid lines* for detected sources, *dotted lines* for upper limits). Only single stars are represented for clarity. We note the existence of X-ray emitters with luminosities 10^{30}–10^{31} ergs s^{-1} located near the track for stars with $\sim 2\ M_\odot$, starting at $B-V \sim 0.7$. These are high X-ray luminosity single G giants (HR 4883, 5889, 6970) on the exit from the Hertzsprung gap. Their main-sequence progenitors should be A stars, which do not show evidence of being strong X-ray emitters (Schmitt *et al.* 1985), most likely because they lack a subphotospheric convection zone, a necessary (though not sufficient) ingredient for dynamo activity. We know that such a convection zone develops just before stars enter the red giant branch, and this may favour the onset of a dynamo mechanism and the heating of the outer atmospheres. Near $B-V \sim 0.4$ we observe instead X-ray sources with $\log L_x \sim 10^{28}$–10^{29} ergs s^{-1}. These are probably low-mass stars ($M \gtrsim 1\ M_\odot$) slightly evolved beyond the main sequence. These stars do show all the signs of magnetic field–related surface activity since their arrival on the main sequence. Their following evolution, with an apparent increase of the X-ray luminosity (see stars with $B-V \sim 0.6$–0.8 near the track for $1.1\ M_\odot$ stars in Fig. 8; see HR 2085, HR 3318, and HR 3771), could be influenced by the increase of the convection zone depth. Finally, near the spectral type G8 III ($B-V \sim 0.9$), the range in X-ray luminosity is too large to be explained simply by differences in the star masses (see § IV*b* for some examples).

If the solar-like dynamo hypothesis is applicable, we would like to recover the rotation-activity relation which holds for late-type main-sequence stars. Pallavicini *et al.* (1981) have empirically established a correlation between the X-ray luminosity, L_x, and the projected rotational velocity, $v \sin i$, using a sample which included six giants also present in our survey (but here considered potential multiple sources). The expectation of a relationship between X-ray luminosity and surface rotation rate derives from the notion, *qualitatively* deduced from theoretical dynamo models, that larger rotation rates should lead to more efficient amplification of magnetic fields via the ω-process (Parker 1979), and from the (solar) empirical observation that increased surface magnetic activity implies increased levels of coronal heating. The theory is at present unable to quantify either of these expected correlations, so that we have—for convenience's sake—just adopted a simple power law between L_x and $v \sin i$ in order to parameterize the rotation-activity relation; this is consistent with choices made in previous studies of main-sequence stars (Pallavicini *et al.* 1981; Micela *et al.* 1985; Schmitt *et al.* 1985; Maggio *et al.* 1987). For present purposes, we have collected projected rotational velocities from a number of sources (see Table 2 for the

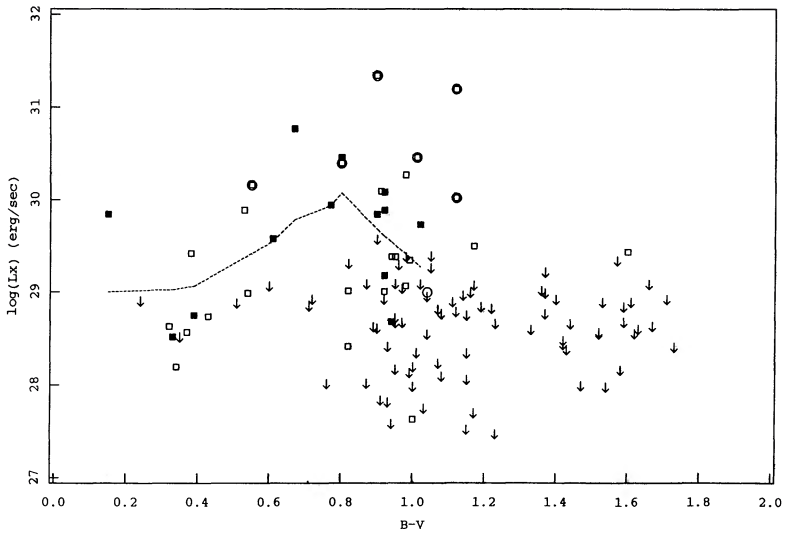

FIG. 7.—X-ray luminosity (0.2–4 keV) vs. $B-V$ color, for all stars within 100 pc. Filled squares are used for detected X-ray sources identified with single stars, empty squares for detected binaries or multicomponent systems, while arrows indicate upper limits on the X-ray luminosity, regardless of multiplicity. RS CVn–like systems are flagged by circled symbols. Dotted line was obtained by applying a robust smoothing on the single star data sample, taking into account both detections and upper limits; the curve extends over the $B-V$ range defined by the bluest and reddest detections: no single star with $B-V \gtrsim 1$ has been detected. The unique detection at $B-V \sim 1.6$ is the spectroscopic binary ϵ Gem (HR 2216). Note the suggested initial increase of X-ray luminosities with $B-V$; note also the wide range in X-ray luminosity in the region occupied by the late G and early K giants ($0.8 \lesssim B-V \lesssim 1.2$).

references), giving precedence to the most recent determinations obtained by deconvolution of line profiles. In Figure 9, we show the dependence of $v \sin i$ on $B-V$ color. Gray (1982) has recently called attention to the sudden drop in rotation rate for stars around G5 III; he suggested that a strong wind-driven magnetic braking may be responsible for the observed behavior. The question arises whether the X-ray luminosity experiences a similar drop, as could be expected if the surface velocity is a good measure of dynamo-related activity. In Figure 10, we show the scatter diagram of log L_x versus log $v \sin i$, restricted to the single stars in our sample within 100 pc. We have searched for a correlation between these two variables by performing a linear regression, using the algorithm of Schmitt *et al.* (1985), which takes into account both measurements and upper limits (in both variables). The best-fit power law (shown as a *dotted curve* in Fig. 10) is given by

$$\log L_x = 1.2 \log (v \sin i) + 27.3 ,$$

with a *low* but significant correlation coefficient of 0.6 (the 68% confidence interval for this coefficient is [0.5,0.7], and the corresponding confidence interval for the slope is [0.9,1.5], obtained by using a bootstrap calculation with 200 replications). This weak result can be attributed to a number of reasons: (i) inhomogeneity of the rotational data (we have estimated an uncertainty of up to a factor of 2 on the relative $v \sin i$ scale; see Pallavicini *et al.* 1981); (ii) our ignorance of the spin

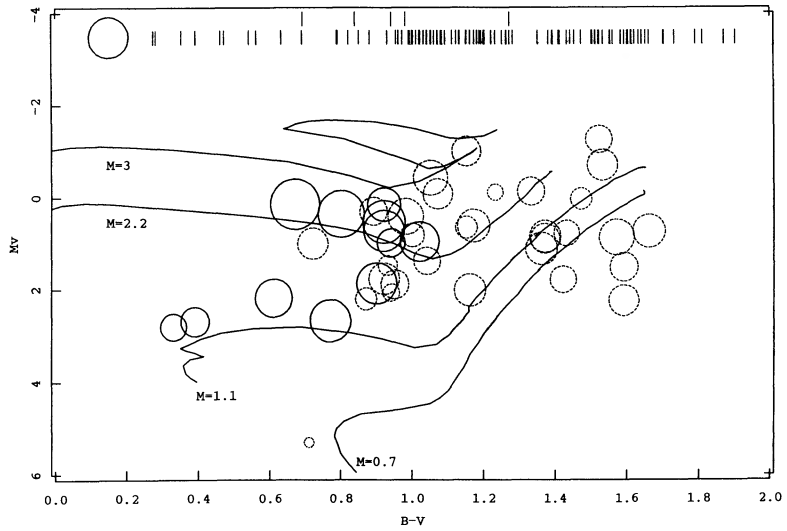

FIG. 8.—An H-R diagram in which X-ray detections (*solid-line circles*) and upper limits (*dotted-line circles*) are plotted as bubbles whose sizes are proportional to log L_x. Only nonbinary stars within 100 pc are represented. Vertical bars on top of the diagram show the $B-V$ distribution of other detections (*upper row*) or nondetections (*lower row*) without available parallax or with distance greater than 100 pc. Superposed evolutionary tracks are the same introduced in Fig. 2. Note the likely low-mass stars near $B-V \sim 0.4$, already detected at an early evolutionary stage.

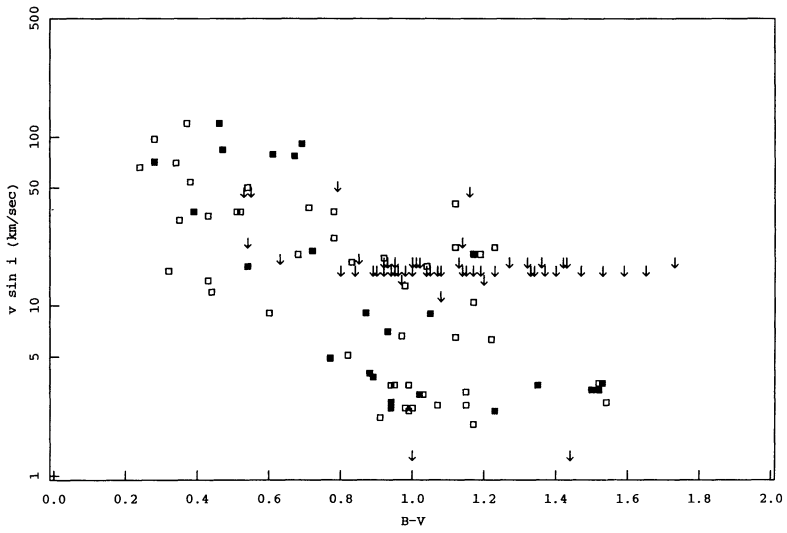

FIG. 9.—Distribution of the projected surface rotational velocity with the $B-V$ color. Squares are used for stars with measured v sin i; filled symbols refer to single stars in our survey, empty symbols to the others. Arrows indicate upper limits on v sin i, regardless of multiplicity. Beyond $B-V \sim 0.8$, most of the stars have surface velocities $\lesssim 10$ km s^{-1}.

axis orientation; (iii) intrinsic variability of the X-ray emission due to rotational modulation or solar-like cycles, to be expected if the magnetic dynamo hypothesis is correct. Nevertheless, our data suggest that no sudden drop in the X-ray emission occurs at the location expected on the basis of the rotational data. In fact, we find that some slowly rotating giants (β Cet, HR 188; 24 UMa, HR 3771) are instead intense X-ray emitters, but we cannot exclude that these stars are viewed nearly pole-on. We have not included the Hyades K0 giants in the luminosity-rotation scatter plot because of their classification as potential binary sources; if we accept that the X-ray emission originates from the giant primary components (see § IV*c*), their position in the log L_x–v sin i diagram would be just below that of β Cet. It is unlikely that the low rotational velocities (v sin $i \sim 2$–3 km^{-1}) of these giants are always due to an high inclination of their spin axes. In conclusion, although the behavior of the giant stars as a whole is in qualitative agreement with the rotation-activity relation followed by the late-type main-sequence stars, the X-ray luminosity is poorly correlated with the surface rotational velocity.

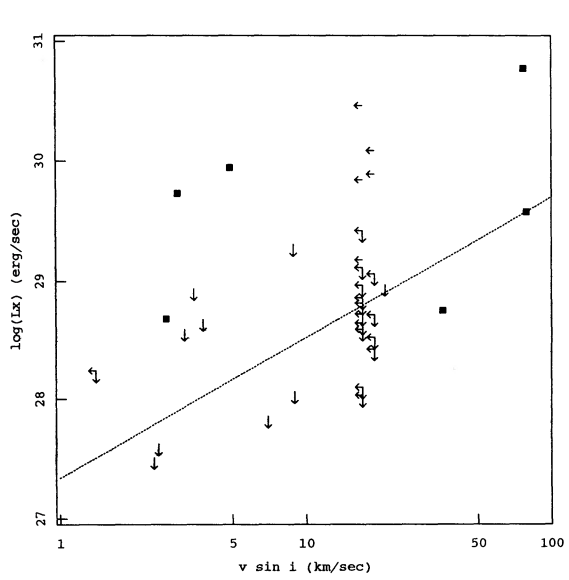

FIG. 10.—Relationship between X-ray luminosity and surface rotational velocity. Squares are used for X-ray detections with available v sin i; arrows indicate stars with upper limits on L_x or v sin i, or both. Best-fit power law has been plotted as a dotted line; correlation coefficient is 0.6. Note the discrepant detections with high X-ray luminosity and low rotational velocity.

We have no definitive explanation for this finding, but we do recall that it is not simply rotation that determines dynamo action, but also differential rotation within the star and the vigor of the Coriolis force acting on turbulent eddies within the convection zone (the α-effect). The observational evidence suggests that for main-sequence stars, the details of the interior rotation structure and effectiveness of the α-effect are not highly relevant to determining the level of surface activity (because the rotation rate, in and of itself, is such an excellent predictor of the activity level). In contrast, it may well be that for giants the differential rotation structure may matter to the point where the rotation rate in and of itself is only a secondary (though highly necessary) determinant of the actual level of surface activity. Following this hypothesis a bit further, we note that any rotational braking should give rise to a radial gradient of the rotation rate (see Gray and Endal 1982). Therefore, although the surface velocity may rapidly decrease with time, the X-ray luminosity may not if the magnetic dynamo is sustained by a large radial differential rotation.

In order to check these ideas further, it would be useful to test the correlation between the X-ray luminosity and the Rossby number, R_0. This parameter, which is the ratio of the rotation period P_{rot} to the convective turnover time τ_c, is also a useful indicator of the efficacy of the α-effect (Durney and Latour 1978; Durney and Robinson 1982). We know from studies of main-sequence stars (Noyes *et al.* 1984; Simon, Herbig, and Boesgaard 1985; Maggio *et al.* 1987), that chromospheric and coronal emission can be well parameterized by the Rossby number. A computation of R_0 for giant stars is not simple, because of the rapid evolution of the stellar interior while the star crosses the Hertzsprung gap, and because of the strong dependence of R_0 on the stellar mass.

Nevertheless, Gilliland (1985) has recently presented a self-consistent computation of R_0 as a function of evolutionary age for stars of 1, 1.3, and 1.6 $M_\odot$, and has shown that the convective turnover time varies by a factor of 6 for a solar-mass star, but over two orders of magnitude for a 1.3 $M_\odot$ star, and over a factor of 3×10^4 for a 1.6 $M_\odot$ star. The Gilliland computation shows that τ_c reaches a maximum near log $T_{\rm eff} \sim 3.7$, with a weak dependence on the star mass. For a given value of the rotation period, a larger value of τ_c yields a smaller Rossby number, which is expected to result in increased production of magnetic fields, and hence more coronal heating and a larger X-ray luminosity. These results suggest that the structural changes in the star interior may have a deep influence on the heating of the outer atmospheres of evolved stars, if powered by a magnetic dynamo. Since rotation is poorly correlated with the X-ray emission for these stars, we speculate that the Rossby number may turn out to be a better indicator of activity for the giants on the active side of the H-R diagram.

d) The Dearth of X-Ray Emission from K and M Giants

Many hypotheses have been proposed to explain the lack of X-ray detections among the red giants. All these theories may be separated into two distinct scenarios: (*a*) the magnetic dynamo is still active, but we do not see X-ray emission because it is not produced or does not reach us; (*b*) the magnetic dynamo is no longer operative, and the structure of the outer atmospheres of red giants is substantially different from the solar case. We can anticipate that X-ray observations alone are not likely to allow us to distinguish between these alternatives because of their poor sensitivity to plasma at temperatures less than 10^6 K. Hence, it is necessary to consider also the chromospheric and transition region emission obtained by means of UV line spectroscopy; we devote a parallel paper (Haisch *et al.* 1988) to the comparison of our X-ray data with the UV data provided by the *IUE* satellite, and in the present context restrict ourselves to discuss the problem of these non–X-ray–emitting stars only in general terms.

There has been considerable effort to establish a link between the failure to detect X-ray emission in red giants and the well-known presence of winds in these stars. Unfortunately, our knowledge of mass-loss rates, terminal velocities, ionization fractions, and isotropy of these flows are far from complete. Most of the observational evidence is consistent with total mass-loss rates of $\sim 10^{-10}$ $M_\odot$ yr^{-1} for early K III stars, increasing to 10^{-8} $M_\odot$ yr^{-1} for mid-M giants (Dupree 1986; Drake and Linsky 1986). Absorption by cool gas in these winds may significantly attenuate the soft X-ray emission originating at the base of the flow. However, the amount of such absorption is only weakly constrained by the simple spherically symmetric and homogeneous flow models we are forced to use. If we assume that the absorption takes place in the flow regime in which the wind is "coasting," so that the wind density falls off with the square of the distance from the star, then one obtains an estimate of the equivalent hydrogen column density of

$$N_{\rm H} = \frac{1}{4\pi m_{\rm H}} \frac{\dot{M}}{R_0 v_w},$$

where $\dot{M}$ is the mass flux, v_w is the wind terminal velocity, and R_0 is the distance above which the flow may be assumed to be "coasting." Since v_w is $\gtrsim 10$ km s^{-1} in the K giants, as derived from the blueshift of UV line absorption components (Stencel, Mullan, and Linsky 1980) or from optical studies of circumstellar features (Boesgaard and Hagen 1979), and the stellar radius is $\gtrsim 10$ $R_\odot$, we estimate that a mass-loss rate of 10^{-10} $M_\odot$ yr^{-1} would be sufficient to produce appreciable absorption of soft X-rays. An optically thin wind may instead result if higher velocities and larger stellar radii are considered, or an exponential decrease of the density near the surface is assumed. In this context, it is relevant to recall our earlier brief discussion of the X-ray spectral analysis. Spectral analysis of the X-ray emission by Schmitt *et al.* (1988) for giant stars as late as $B-V \sim 1.1$ was unable to find evidence of strong absorption in the region in which these winds start to be detected. Although this analysis is necesssarily biased toward stars with large observed X-ray fluxes, and hence may have selected stars with the least amount of self-absorption, a preliminary analysis of the X-ray spectral hardness for a larger sample of stars does not support the idea that X-ray emission from red giants is more absorbed than for typical F and G giants.

The hypothesis that wind energy losses take the place of the radiative emission from transition regions and coronae has been criticized recently by Antiochos, Haisch, and Stern (1986), who stressed how misleading it could be to consider the transition region dividing line as necessarily an indication of the onset of winds. The energy fluxes deduced for the winds of the K giants are of the order 10^5 ergs cm^{-2} s^{-1} (MacGregor 1983), comparable to those required by the solar wind (Withbroe and Noyes 1977). Most likely, the X-ray–emitting G giants also have winds of this energy, which are not easily observable because they are hot ($T \gtrsim 10^5$ K), and do not give rise to spectroscopic effects detectable at UV or longer wavelengths.

Antiochos, Haisch, and Stern (1986) have suggested an alternative to the wind hypothesis, in the context of their "cool loop" model. This model is based on the numerical solution of the static coronal loop equations (Antiochos and Noci 1986): if the pressure scale height ($H_g = kT/mg$ at the temperature corresponding to the peek of the radiative loss function ($T \sim 10^5$K) is greater than the loop height H_l, only one *stable* solution of these equations exists, resulting in a maximum plasma temperature of $T < 10^5$ K (this is the "cool loop" solution). In contrast, if $H_l \gg H_g$, only a hot solution exists, with $T_{\rm max} \gtrsim 10^6$ K (Serio *et al.* 1981). During the stellar evolution toward the giant phase, H_g increases up to a factor 10^4 because of the drop in the surface gravity; the cool solutions may become the only possible solution, and a decrease of the X-ray emission is therefore expected. Note that an increase of the UV versus X-ray flux ratio is predicted and may be testable (Haisch *et al.* 1988).

VI. SUMMARY

We have investigated the behavior of the X-ray emission from late-type evolved stars using an extensive sample of optical candidates (10 times larger than any previously studied sample), and taking advantage of statistical techniques well suited to deal with X-ray data, including many upper limits. Our principal results may be summarized as follows:

1. The observed F giants or subgiants (slightly evolved stars with $M \lesssim 2$ $M_\odot$) are X-ray emitters at the same level of main-sequence stars of similar spectral type ($10^{28} < L_x \lesssim 4 \times 10^{29}$ ergs s^{-1}).

2. The G giants show a range of emission more than three orders of magnitude wide. Some presumed single G giants exist with X-ray luminosities comparable to RS CVn systems ($L_x \gtrsim 10^{30}$ ergs s^{-1}), while some nearby late G giants have upper limits on the X-ray emission below typical solar values ($L_x \lesssim$ a

few $\times 10^{27}$ ergs s^{-1}). The mean X-ray luminosity for the single G giants is about a factor 10 higher than for G main-sequence field stars. The wider range of X-ray emission for the G giants with respect to the F giants is likely related to the larger spread in masses and evolutionary states of the fomer star sample.

3. K giants have an observed X-ray emission level significatively lower than F and G giants (median $L_x \lesssim 10^{28}$ ergs s^{-1}). Most sources are identified with multicomponent systems, but the K0 giants are probably X-ray emitters with X-ray luminosity comparable to the G giants, and to the young-disk K dwarfs.

4. M giants and F–M supergiants have been sampled with relatively lower sensitivities in this survey because of their large distances. We can only state that their median X-ray luminosity must be lower than $\sim 10^{29}$ ergs s^{-1}. Moreover, the data at hand are not able to establish a statistically significant difference between the X-ray emission levels of giant and supergiant stars.

5. Inactive main-sequence stars, like A dwarfs, develop an efficient magnetic dynamo while crossing the Hertzsprung gap, likely favored by the onset of a surface convection zone. The X-ray observations alone are not able to discriminate between the various models proposed to explain the lack of detections among the red giant stars.

6. The surface rotational velocity is not a good indicator of the X-ray luminosity level for the giant stars. We believe that other parameters linked to the properties of the stellar convection zone and to the internal differential rotation would be more useful for this purpose, at least in the region with $B - V \lesssim 1$.

We would like to thank G. Micela, S. Sciortino, and Professor S. Serio for useful discussions on our manuscript, and the following agencies for partial financial support of the work reported here: NASA (through contract NAS8-30751 [F. R. H.] and grant NAGW-112 [J. B.] to the Smithsonian Astrophysical Observatory, through grant NAGW-1716 to the University of Colorado [J. B.], and H-89765B to the Lockheed Palo Alto Research Laboratories [B. H.]), the Lockheed Independent Research Program [R. S.], and the Italian CNR, MPI, and CRRNSM [A. M., G. S. V.]. We also like to thank the anonymous referee of this paper.

REFERENCES

Allen, C. W. 1973, *Astrophysical Quantities* (3d ed.; London: Athlone).
Alschuler, W. R. 1975, *Ap. J.*, **195**, 649.
Antiochos, S., Haisch, J. L., and Stern, R. A. 1986, *Ap. J. (Letters)*, **307**, L55.
Antiochos, S., and Noci, G. 1986, *Ap. J.*, **301**, 440.
Ayres, T. R., Linsky, J. L., Vaiana, G. S., Golub, L., and Rosner, R. 1981, *Ap. J.*, **250**, 293.
Ayres, T. R., Simon, T., and Linsky, 1982, *Ap. J.*, **263**, 791.
Bahcall, J. N., Casertano, S., and Ratnatunga, K. U. 1987, *Ap. J.*, **320**, 515.
Baliunas, S. L., Hartmann, L., and Dupree, A. K. 1983, *Ap. J.*, **271**, 672.
Becker, S. A. 1981, *Ap. J. Suppl.*, **45**, 475.
Böhm-Vitense, E. 1986, *Ap. J.*, **301**, 297.
Boesgaard, A. M., and Hagen, W. 1979, *Ap. J.*, **231**, 128.
Bookbinder, J. 1985, Ph.D. thesis, Harvard University.
Cleveland, W. S. 1979, *J. Am. Stat. Ass.*, **74**, 829.
Drake, S. A., and Linsky, J. L. 1986, *A.J.*, **91**, 602.
Dupree, A. K. 1986, *Ann. Rev. Astr. Ap.*, **24**, 377.
Durney, B. R., and Latour, J. 1978, *Geophys. Ap. Fluid Dyn.*, **9**, 241.
Durney, B. R., and Robinson, R. D. 1982, *Ap. J.*, **253**, 290.
Efron, B. 1982, *The Jacknife, the Bootstrap, and Other Resampling Plans* (Philadelphia: SIAM).
Eggen, O. J. 1969, *Pub. A.S.P.*, **81**, 353.
Endal, A. S. 1983, in *IAU Symposium 102, Solar and Magnetic Fields: Origins and Coronal Effects*, ed. J. O. Stenflo (Dordrecht: Reidel), p. 493.
Faber, S. M., Friel, E. D., Burstein, D., and Gaskell, C. M. 1985, *Ap. J. Suppl.*, **57**, 711.
Favata, F., Rosner, R., Sciortino, S., and Vaiana, G. S. 1988, *Ap. J.*, **324**, 1010.
Feigelson, E. D., and Nelson, P. I. 1985, *Ap. J.*, **293**, 192.
Flower, P. J. 1977, *Astr. Ap.*, **54**, 31.
Gehrels, N. 1986, *Ap. J.*, **303**, 336.
Giacconi, R., *et al.* 1979, *Ap. J.*, **230**, 540.
Gilliland, R. L. 1985, *Ap. J.*, **299**, 286.
Gondoin, P., Mangenay, A., and Praderie, F. 1987, *Astr. Ap.*, **174**, 187.
Gorenstein, P., Harnden, F. R., Jr., and Fabricant, D. G. 1981, *IEEE Trans. Nucl. Sci.*, **NS-28**, 869.
Gray, D. F. 1982, *Ap. J.*, **262**, 682.
Gray, D. F., and Endal, A. S. 1982, *Ap. J.*, **254**, 162.
Gray, D. F., and Nagar, P. 1985, *Ap. J.*, **298**, 756.
Gray, D. F., and Toner, C. G. 1986, *Ap. J.*, **310**, 277.
Haisch, B. M. 1986, *Irish A. J.*, **17**, 200.
———. 1987, in *Lecture Notes in Physics*, Vol. **291**, *Cool Stars, Stellar System, and the Sun*, ed. J. M. Linsky and R. E. Stencel (New York: Springer), p. 269.
Haisch, B. M., Bookbinder, J., Maggio, A., Vaiana, G. S., Harnden, F. R., Jr., Rosner, R., and Bennett, J. O. 1989, in preparation.
Haisch, B. M., and Simon, T. 1982, *Ap. J.*, **263**, 252.
Harnden, F. R., Jr., Fabricant, D. G., Harris, D. E., and Schwartz, J. 1984, *Smithsonian Ap. Obs. Spec. Rept.*, No. 393.
Harnden, F. R., Jr., Sciortino, S., Maggio, A., Micela, G., Vaiana, G. S., and Schmitt, J. 1989, in *From Einstein to AXAF*, ed. M. Elvis and T. Maccacaro (Cambridge: Cambridge University Press), in press.
Harris, D. E., and Irwin, D. 1984, *Einstein Observatory Revised User's Manual.*
Hartmann, L., Dupree, A. K., and Raymond, J. C. 1980, *Ap. J. (Letters)*, **236**, L143.
Herbig, G., and Spalding, J. 1955, *Ap. J.*, **121**, 118.
Hoffleit, D., and Jaschek, C. 1982, *The Bright Star Catalogue* (New Haven: Yale University Press).
Hoffleit, D., Saladyga, M., and Wlasuk, P. 1984, *A Supplement to the Bright Star Catalog* (New Haven: Yale University Press).
Iben, I., Jr. 1967, *Ann. Rev. Astr. Ap.*, **5**, 571.
Johnson, H. L. 1966, *Ann. Rev. Astr. Ap.*, **4**, 193.
Linsky, J. L., and Haisch, B. M. 1979, *Ap. J. (Letters)*, **229**, L27.
Maccacaro, T., *et al.* 1982, *Ap. J.*, **253**, 504.
MacGregor, K. B. 1983, in *Solar Wind Five*, ed. M. Neugebauer (NASA CP-2280), p. 241.
Maggio, A., Sciortino, S., Bookbinder, J., Harnden, F. R., Jr., Golub, L., Majer, P., Rosner, R., and Vaiana, G. S. 1987, *Ap. J.*, **315**, 687.
Majer, P., Schmitt, J. H. M. M., Golub, L., Harnden, F. R., Jr., and Rosner, R. 1985, *Ap. J.*, **300**, 360.
Mengel, J. G., Sweigart, A. V., Demarque, P., and Gross, P. G. 1979, *Ap. J. Suppl.*, **40**, 733.
Micela, G., Sciortino, S., Serio, S., Vaiana, G. S., Bookbinder, J., Golub, L., Harnden, F. R., Jr., and Rosner, R. 1985, *Ap. J.*, **292**, 172.
Micela, G., Sciortino, S., Vaiana, G. S., Schmitt, J. H. M. M., Stern, R. A., Harnden, F. R., Jr., and Rosner, R. 1988, *Ap. J.*, **325**, 798.
Noyes, R. W., Hartmann, L. W., Baliunas, S. L., Duncan, D. K., and Vaughan, A. H. 1984, *Ap. J.*, **279**, 763.
Pallavicini, R., Golub, L., Rosner, R., Vaiana, G. S., Ayres, T., and Linsky, J. L. 1981, *Ap. J.*, **248**, 279.
Parker, E. N. 1979, *Cosmical Magnetic Fields* (Oxford: Clarendon).
Raymond, J. C., and Smith, B. W. 1977, *Ap. J. Suppl.*, **35**, 419.
Reimers, D. 1977, *Astr. Ap.*, **57**, 395.
Rosner, R., Golub, L., and Vaiana, G. S. 1985, *Ann. Rev. Astr. Ap.*, **23**, 413.
Rutten, R. G. M., and Pylyser, E. 1988, *Astr. Ap.*, **191**, 227.
Schmitt, J. H. M. M. 1985, *Ap. J.*, **293**, 178.
Schmitt, J. H. M. M., Collura, A., Sciortino, S., Vaiana, G. S., Harnden, F. R., Jr., and Rosner, R. 1989, in preparation.
Schmitt, J. H. M. M., Golub, L., Harnden, F. R., Jr., Maxon, C. W., Rosner, R., and Vaiana, G. S. 1985, *Ap. J.*, **290**, 307.
Sciortino, S., Harnden, F. R., Jr., Maggio, A., Micela, G., Vaiana, G. S., Schmitt, J., and Rosner, R. 1988, in *Astronomy from Large Databases*, ed. F. Murtagh and A. Heck (ESO Conf. and Workshop Proc. No. 28).
Serio, S., Peres, G., Vaiana, G. S., Golub, L., and Rosner, R. 1981, *Ap. J.*, **243**, 288.
Simon, T. 1984, *Ap. J.*, **279**, 738.
Simon, T., Herbig, G., and Boesgaard, A. M. 1985, *Ap. J.*, **293**, 553.
Simon, T., Linsky, J. L., and Stencel, R. E. 1982, *Ap. J.*, **257**, 225.
Stencel, R. E. 1978, *Ap. J. (Letters)*, **223**, L37.
Stencel, R. E., and Mullan, D. J. 1980, *Ap. J.*, **238**, 221.
Stencel, R. E., Mullan, D. J., and Linsky, J. L. 1980, *Ap. J. Suppl.*, **44**, 383.

Strassmeier, K. G., Hall, D. S., Zeilik, M., Nelson, E., Eker, Z., and Fekel, F. C. 1988, *Astr. Ap. Suppl.*, **72**, 291.
Sweigart, A. V., and Gross, P. G. 1978, *Ap. J. Suppl.*, **36**, 405.
Vaiana, G. S., *et al.* 1981, *Ap. J.*, **245**, 163.
Vaiana, G. S., and Sciortino, S. 1986, *Adv. Space Res.*, **6**, 99.
Walter, F. M., and Bowyer, S. 1981, *Ap. J.*, **245**, 671.
Walter, F. M., Gibson, D. M., and Basri, G. S. 1983, *Ap. J.*, **267**, 665.
Withbroe, J. L., and Noyes, R. W. 1977, *Ann. Rev. Astr. Ap.*, **15**, 363.

J. BOOKBINDER and F. R. HARNDEN, JR.: Harvard-Smithsonian Center for Astrophysics, 60 Garden Street, Cambridge, MA 02138

B. M. HAISCH and R. A. STERN: Lockheed Palo Alto Research Laboratory, 3251 Hanover Street, Palo Alto, CA 94304

A. MAGGIO and G. S. VAIANA: Osservatorio Astronomico di Palermo, Palazzo dei Normanni, 90134 Palermo, Italy

R. ROSNER: Department of Astronomy and Astrophysics and Enrico Fermi Institute, University of Chicago, IL 60637